Luminescence in the Solid State of Phosphine-EWO Ligands with Fluorinated Chalcone Skeletons and their PdX_2 complexes. Metal-promoted Phosphorescence Enhancement

Jaime Ponce-de-León,[a] Marconi N. Peñas-Defrutos,[a,*] Andrea Vélez,[a] Gabriel Aullón,[b] and Pablo Espinet[a,*]

[a] IU CINQUIMA/Química Inorgánica, Facultad de Ciencias, Universidad de Valladolid, 47071-Valladolid (Spain)

[b] Departament de Química Inorgànica, Universitat de Barcelona, Martí i Franquès 1-11, E-08028 Barcelona, (Spain).

**To whom correspondence should be addressed:*

marconi_44@hotmail.com, espinet@qi.uva.es

Table of Content

General Experimental Section 1

Synthesis of iPr-PEWO-F_4 (**L^3**) 2

(2-bromo-3,4,5,6-tetrafluorophenyl)diisopropylphosphine 2

2-(diisopropylphosphaneyl)-3,4,5,6-tetrafluorobenzaldehyde 2

iPr-PEWO-F_4 (**L^3**) 2

Synthesis of Organometallic Complexes 3

General procedure for the synthesis of trans-$PdCl_2(L^{2-3})_2$ complexes 3

trans-[$PdCl_2$(Cy-PEWO-F_4)$_2$] (**$1L^2$**) 3

trans-[$PdCl_2$(iPr-PEWO-F_4)$_2$] (**$1L^3$**) 3

trans-[$PdBr_2$(Ph-PEWO-F_4)$_2$] (**$3L^1$**) 4

trans-[$Pd(CN)_2$(Ph-PEWO-F_4)$_2$] (**$4L^1$**) 4

trans-[$PtCl_2$(Ph-PEWO-F_4)$_2$] (**$5L^1$**) 5

X-ray Crystallographic Data 6

Photophysical Properties 10

Emission Spectra 11

Luminescence Data 12

Emission Decay Profiles 13

Excitation Spectra 17

DFT Calculations 18

Computational details 18

Absorption spectra 18

Phosphorescence emission 27
Fluorescence emission 30
NMR Spectra 32
Fluxionality of **1L^2** and **1L^3** complexes 44
References 45

General Experimental Section

All the manipulations were performed by standard Schlenk techniques under N_2 atmosphere. Solvents were dried using a solvent purification system SPS PS-MD-5 or distilled from appropriate drying agents,[1] and were sparged with nitrogen gas. Solvents for experiments in an inert atmosphere were stored into flame-dried Schlenk flasks over freshly activated 3 or 4 Å molecular sieves.

Commercially available chemicals were purchased from Sigma Aldrich, Alfa Aesar, Fluorochem and Acros Organics and were used without further purification.

Ph-PEWO-F_4 (**L^1**), $PdCl_2$(Ph-PEWO-F_4) (**2L^1**) and $PdCl_2$(Ph-PEWO-F_4)$_2$ (**1L^1**), [2] Cy-PEWO-F_4 (**L^2**),[3] Ph-PEWO-H_4 (**L^4**),[4] and $PdCl_2$(Ph-PEWO-H_4)$_2$ (**1L^4**),[5] were prepared by reported methods. Flash chromatography was carried out using silica gel (230-240 mesh). Chemical yields refer to pure isolated substances.

NMR spectra were recorded with Varian 500/54 Premium Shielded instruments. Chemical shifts are reported in ppm referenced to tetramethylsilane (^{1}H), CCl_3F (^{19}F), and 85% H_3PO_4 (^{31}P), with positive shifts downfield, at 298 K. Coupling constants (*J*) are given in hertz (Hz). The following abbreviations are used to describe peak patterns when appropriate: s (singlet), d (doublet), t (triplet), m (multiplet) and br (broad).

Elemental analysis were carried out with Elemental Analyser EA Flash 2000 (Thermo Fisher Scientific at the PCT facilities of the University of Burgos (Spain).

Luminescence studies were carried out at the PCT facilities of the University of Burgos (Spain). All measurements were carried out under air. Steady–state fluorescence measurements were carried out by using a FLS980 fluorescence spectrometer with a 450W Xe lamp as a light source and double excitation and emission monochromators. Monochromator at 400 nm was used at the excitation and emission arms. A photomultiplier tube detector cooled by a Peltier system was used for detection. To measure the emission lifetimes and photoluminescence quantum yield (QY) the FLS980 fluorescence spectrometer is equipped with an integrating sphere. All data were measured at 25 °C. Time-resolved fluorescence measurements were carried out using the single-photon counting technique with ns time resolution. A high repletion pulsed light source is used to excite the sample and the photons emitted are processed using the TCC1 card in the computer. Fluorescence decays were obtained with the Time Correlated Single Photon Counting (TCSPC) and MCP-PMT counter module (TCC2) of the FLS980 spectrometer (Edinburgh Instruments). Fluorescence decays were analysed with the method of non-linear least squares iterative deconvolution ant the quality of the fits was judged by the values of the reduced Chi-square (χ^2) and the autocorrelation function of the residuals using the FAST (Advanced Fluorescence Lifetime Analysis Software) programme provided by the equipment.

Synthesis of iPr-PEWO-F_4 (L^3)

iPr-PEWO-F_4 (**L^3**) was synthetised following a literature procedure for the general synthesis of R-PEWO-F_4 ligands (Scheme S1),[3] employing iPr_2PCl. **L^3** was obtained in a 58.0 % global yield.

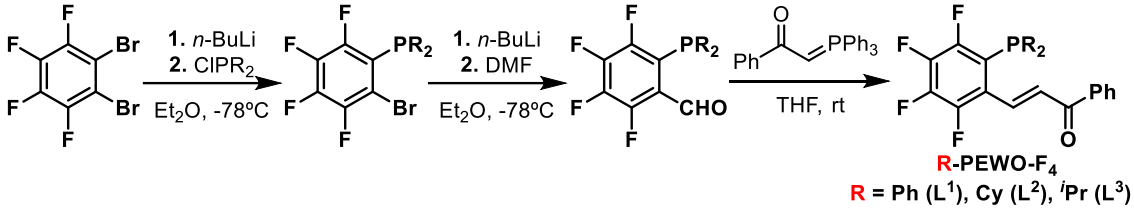

Scheme S1. General synthesis for R-PEWO-F_4 (**L^1**-**L^3**)

(2-bromo-3,4,5,6-tetrafluorophenyl)diisopropylphosphine

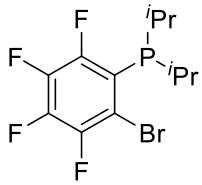

Product was isolated as a colourless solid (90.0 % yield).

Elemental analysis. $C_{12}H_{14}BrF_4P$. Calculated %: C, 41.76; H, 4.09. Experimental %: C, 41.78; H, 4.11.

^{1}H NMR (499.72 MHz, Chloroform-*d*) δ 2.51 (dttt, *J* = 12.5, 7.0, 3.7, 1.9 Hz, 2H), 1.19 (dd, *J* = 17.2, 6.9 Hz, 6H), 0.96 (ddd, *J* = 12.5, 7.0, 1.2 Hz, 6H).

^{19}F NMR (470.17 MHz, Chloroform-*d*) δ -124.60 – -124.80 (m), -124.91 (dtd, *J* = 21.3, 10.1, 3.4 Hz), -150.47 (td, *J* = 20.8, 5.5 Hz), -154.95 (ddt, *J* = 23.3, 19.6, 3.4 Hz).

^{31}P{^{1}H} NMR (202.30 MHz, Chloroform-*d*) δ 25.0 (dd, *J* = 8.6, 8.0 Hz).

2-(diisopropylphosphaneyl)-3,4,5,6-tetrafluorobenzaldehyde

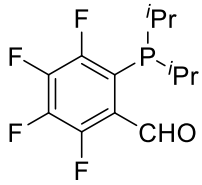

Formation of aldehyde was confirmed by ^{1}H NMR. Product was used in the next step without further purification.

^{1}H NMR (499.72 MHz, Chloroform-*d*) δ 10.51 (dd, *J* = 6.9, 2.0 Hz, 1H).

^{19}F NMR (470.17 MHz, Chloroform-*d*) δ -119.35 – -123.16 (m), -141.75 – -144.86 (m), -143.68 – -146.15 (m), -150.44 (td, *J* = 19.9, 7.3 Hz).

^{31}P{^{1}H} NMR (202.30 MHz, Chloroform-*d*) δ 0.8 (dt, *J* = 18.2, 2.7 Hz).

iPr-PEWO-F_4 (L^3)

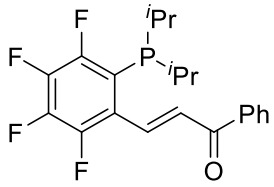

Elemental analysis. $C_{21}H_{21}F_4OP$. Calculated %: C, 63.64; H, 5.34. Experimental %: C, 63.65; H, 5.34.

^{1}H NMR (499.72 MHz, Chloroform-*d*) δ 8.47 (dd, *J* = 16.1, 5.5 Hz, 1H), 8.03 (d, *J* = 7.7 Hz, 2H), 7.68 – 7.46 (m, 4H), 2.57 – 2.44 (m, 2H), 1.14 (dd, *J* = 17.5, 6.9 Hz, 6H), 0.92 (dd, *J* = 12.4, 7.0 Hz, 6H).

^{19}F NMR (470.17 MHz, Chloroform-*d*) δ -125.28 – -125.54 (m), -136.37 – -136.55 (m), -152.49 (td, *J* = 20.1, 5.8 Hz), -152.75 (ddt, *J* = 24.0, 19.9, 3.9 Hz).

^{31}P{^{1}H} NMR (202.30 MHz, Chloroform-*d*) δ 7.1 (dt, *J* = 20.0, 3.7 Hz).

Synthesis of Organometallic Complexes

General procedure for the synthesis of trans-$PdCl_2(L^{2-3})_2$ complexes

In a flame-dried Schlenk flask, the corresponding ligand **L^2** or **L^3** (0.79 mmol, 2.05 eq) was added to an orange suspension of *trans*-$[PdCl_2(CH_3CN)_2]$ (100.0 mg, 0.38 mmol) in CH_2Cl_2 (10 mL), and after a few minutes the resulting mixture turn off to a yellowish solution. After stirring for 30 min at room temperature, the solution was filtered through Celite and evaporated to dryness. *n*-hexane was added to afford a yellow solid, which was washed with Et_2O (2 × 4mL) and *n*-hexane (2 × 4 mL) and dried in vacuum

trans-$[PdCl_2(Cy\text{-}PEWO\text{-}F_4)_2]$ ($1L^2$)

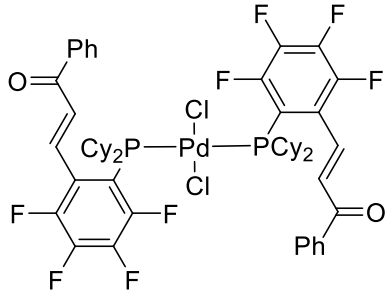

Prepared following general procedure employing Cy-PEWO-F_4 as ligand. Product was obtained as a yellow solid (87.1 % yield)

X-ray-quality crystals were grown by slow diffusion of an acetone/*n*-hexane mixture at –20 °C.

Elemental analysis. $C_{54}H_{58}Cl_2F_8O_2P_2Pd$. Calculated %: C, 57.38; H, 5.17. Experimental %: C, 57.41; H, 5.15.

^{1}H NMR (499.72 MHz, Chloroform-*d*) δ 8.17 (br, 2H), 8.02 (dd, *J* = 8.3, 1.2 Hz, 4H), 7.61 (tt, *J* = 7.4, 7.3, 1.9 Hz, 2H), 7.57 – 7.42 (m, 6H), 2.84 (t, *J* = 12.1 Hz, 4H), 2.22 (d, *J* = 12.3 Hz, 4H), 1.85 (t, *J* = 15.1 Hz, 8H), 1.64 (ddd, *J* = 71.4, 45.8, 27.4 Hz, 16H), 1.36 (tdd, *J* = 13.0, 9.4, 3.2 Hz, 4H), 1.25 – 1.05 (m, 8H).

^{19}F NMR (470.17 MHz, Chloroform-*d*) δ -136.23 (br), -149.81 (td, *J* = 21.2, 8.1 Hz), -152.08 (br).

^{31}P{^{1}H} NMR (202.30 MHz, Chloroform-*d*) δ 30.5 (s).

trans-$[PdCl_2(iPr\text{-}PEWO\text{-}F_4)_2]$ ($1L^3$)

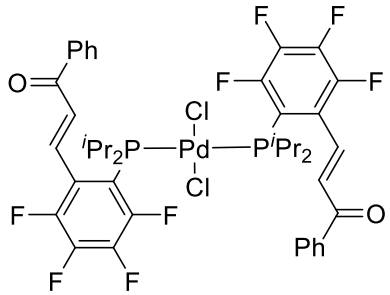

Prepared following general procedure employing iPr-PEWO-F_4 (**L^3**) as ligand. Product was obtained as a yellow solid (84.6 % yield).

X-ray-quality crystals were grown by slow diffusion of a CH_2Cl_2/*n*-hexane mixture at –20 °C.

Elemental analysis. $C_{39}H_{35}Cl_2F_8O_2P_2Pd$. Calculated %: C, 48.90; H, 3.68. Experimental %: C, 48.91; H, 3.67.

^{1}H NMR (499.72 MHz, Chloroform-*d*) δ 8.34 (br, 1H), 8.01 (d, J = 7.3 Hz, 2H), 7.64 – 7.54 (m, 1H), 7.50 (t, J = 7.8 Hz, 2H), 3.07 (p, J = 7.2 Hz, 2H), 1.41 (q, J = 8.7 Hz, 6H), 1.26 (q, J = 7.6 Hz, 6H).

^{19}F NMR (470.17 MHz, Chloroform-*d*) δ -134.82 (br), -149.42 (dt, *J* = 23.5, 11.9 Hz), -152.12 (t, *J* = 21.8 Hz).

^{31}P{^{1}H} NMR (202.30 MHz, Chloroform-*d*) δ 42.0 (s).

trans-[$PdBr_2$(Ph-PEWO-F_4)$_2$] (3L^1)

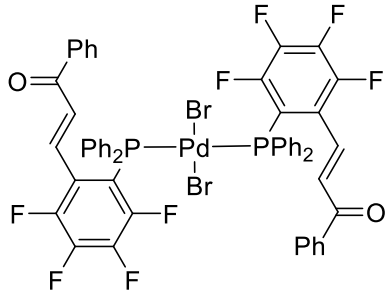

In a round bottom flask, *trans*-[$PdCl_2$(Ph-PEWO-F_4)$_2$] (**1L^1**) (50.7 mg, 45.8 µmol) and KBr (57,4 mg, 482 µmol) were dissolved in 8 mL of acetone. The solution was stirred at room temperature for 1 hour and taken to dryness under vacuum. The solid obtained was redissolved in CH_2Cl_2 and filtered through Celite. The filtrate was taken to dryness obtaining the product as a yellow solid. It was washed with Et_2O (2 x 5 mL) and dried under vacuum. Yellow solid (47.2 mg, 86.3 % yield).

Elemental analysis. $C_{54}H_{34}Br_2F_8O_2P_2Pd$. Calculated %: C, 54.27; H, 2.87. Experimental %: C, 54.34; H, 2.90

^{1}H NMR (499.72 MHz, Chloroform-*d*) δ 8.01 – 7.88 (m, 8H), 7.78 (dt, *J* = 8.3, 1.1 Hz, 4H), 7.68 (d, *J* = 15.7 Hz, 2H), 7.55 (t, *J* = 7.1 Hz, 2H), 7.42 (t, *J* = 7.6 Hz, 4H), 7.38 – 7.30 (m, 12H), 7.09 (d, *J* = 15.3 Hz, 2H).

^{19}F NMR (470.17 MHz, Chloroform-*d*) δ -120.25 – -120.69 (m), -136.23 – -136.45 (m), -150.03 (td, *J* = 20.7, 7.1 Hz), -152.43 (t, *J* = 21.5 Hz).

^{31}P{^{1}H} NMR (202.30 MHz, Chloroform-*d*) δ 14.9 (s).

trans-[$Pd(CN)_2$(Ph-PEWO-F_4)$_2$] (4L^1)

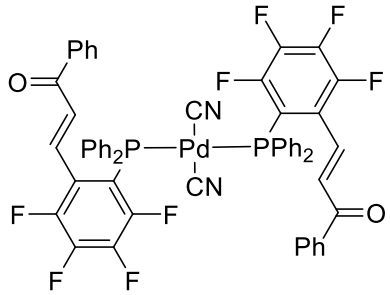

In a round bottom flask, 5 mL of water were added to a mixture of $AgNO_3$ (35.5 mg, 209 µmol) and KCN (13.7 mg, 210 µmol) in the absence of light. The solution was stirred at room temperature for 2 hours. Then, 5 mL of acetone and *trans*-[$PdCl_2$(Ph-PEWO-F_4)$_2$] (**1L^1**) (110.0 mg, 99.4 µmol) were added and the mixture was stirred for 1 hour. The solution was concentrated under vacuum and extracted with CH_2Cl_2 (3 x 5 mL). The organic phase was filtered through Celite and taken to dryness. The solid obtained was washed with Et_2O and dry under vacuum. The title product was obtained as an off-white solid (71.8 mg, 66.5 % yield).

X-ray-quality crystals were grown by slow diffusion of a CH_2Cl_2/*n*-hexane mixture at –20 °C.

Elemental analysis. $C_{56}H_{34}F_8N_2O_2P_2Pd$. Calculated %: C, 61.86; H, 3.15; N, 2.58. Experimental %: C, 61.69; H, 3.17; N, 2.67

^{1}H NMR (499.72 MHz, Chloroform-*d*) δ 7.87 (qd, *J* = 7.1, 6.5, 1.7 Hz, 8H), 7.73 (dd, *J* = 8.1, 1.4 Hz, 4H), 7.59 – 7.50 (m, 2H), 7.46 – 7.38 (m, 16H), 7.36 (d, *J* = 15.7 Hz, 2H), 7.13 (dd, *J* = 15.7, 1.6 Hz, 2H).

^{19}F NMR (470.17 MHz, Chloroform-*d*) δ -120.36 (dp, *J* = 18.7, 9.4 Hz), -135.08 – -135.26 (m), -147.73 (td, *J* = 20.8, 8.1 Hz), -151.35 (t, *J* = 20.1 Hz).

$^{31}P\{^{1}H\}$ NMR (202.30 MHz, Chloroform-*d*) δ 15.4 (s).

trans-[$PtCl_2$(Ph-PEWO-F_4)$_2$] (5L^1)

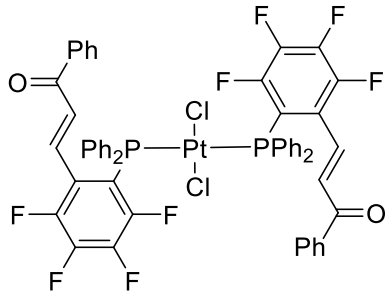

In a flame-dried Schlenk flask, *trans*-[$PtCl_2(CH_3CN)_2$] (100.0 mg, 0.38 mmol) and Ph-PEWO-F_4 (0.79 mmol, 2.05 eq) were dissolved in 10 mL of CH_2Cl_2 at room temperature. The solution was stirred for 1 hour, *n*-hexane (10 mL) was added to induce precipitation of the product and the solvent was removed under vacuum. The yellow solid obtained was sonicated with Et_2O, filtered under air and washed with Et_2O (2 x 5 mL). It was dried under vacuum affording the title compound as an off-white solid.

X-ray-quality crystals were grown by slow diffusion of a CH_2Cl_2/*n*-hexane mixture at –20 °C.

Elemental analysis. $C_{54}H_{34}Cl_2F_8O_2P_2Pt$. Calculated %: C, 54.29; H, 2.87. Experimental %: C, 54.44; H, 2.81

^{1}H NMR (499.72 MHz, Chloroform-*d*) δ 8.15 – 8.03 (m, 8H), 7.82 (d, *J* = 15.8 Hz, 2H), 7.79 – 7.70 (m, 4H), 7.57 – 7.50 (m, 2H), 7.44 – 7.32 (m, 16H), 6.99 (dd, *J* = 15.8, 1.9 Hz, 2H).

^{19}F NMR (470.17 MHz, Chloroform-*d*) δ -122.59 – -123.20 (m), -136.78 (dd, *J* = 24.1, 11.3 Hz), -149.94 (td, *J* = 20.8, 7.1 Hz), -152.70 (t, *J* = 19.1 Hz).

$^{31}P\{^{1}H\}$ NMR (202.30 MHz, Chloroform-*d*) δ 14.7 (d, $J_{Pt\text{-}P}$ = 2734.3 Hz), 14.7 (s).

X-ray Crystallographic Data

A crystal was attached to a glass fiber and transferred either to an Agilent Supernova diffractometer with an Atlas CCD area detector (Valladolid University facilities). The crystal was kept at 294 K or 210 K during data collection. Data collection was performed with Mo-Kα radiation (λ = 0.71073 Å). Data integration, scaling and empirical absorption correction were carried out using the CrysAlisPro program package.[6] Using Olex2,[7] the structure was solved with the ShelxT structure solution program,[8] and refined with ShelxL program.[9] The non-hydrogen atoms were refined anisotropically and hydrogen atoms were placed at idealized positions and refined using the riding model. Refinement proceeded smoothly to give the residuals shown in Table S1 and Table S2. CCDC 2205013-2205017 contains the supporting crystallographic data for this paper. These data can be obtained free of charge at www.ccdc.cam.ac.uk/conts/retrieving.html [or from the Cambridge Crystallographic Data Centre, 12, Union Road, Cambridge CB2 1EZ, UK; fax: (internat.) +44-1223/336-033; E-mail: deposit@ccdc.cam.ac.uk]. Figure 3, Figure S1 and Figure S2 show the molecular structures obtained.

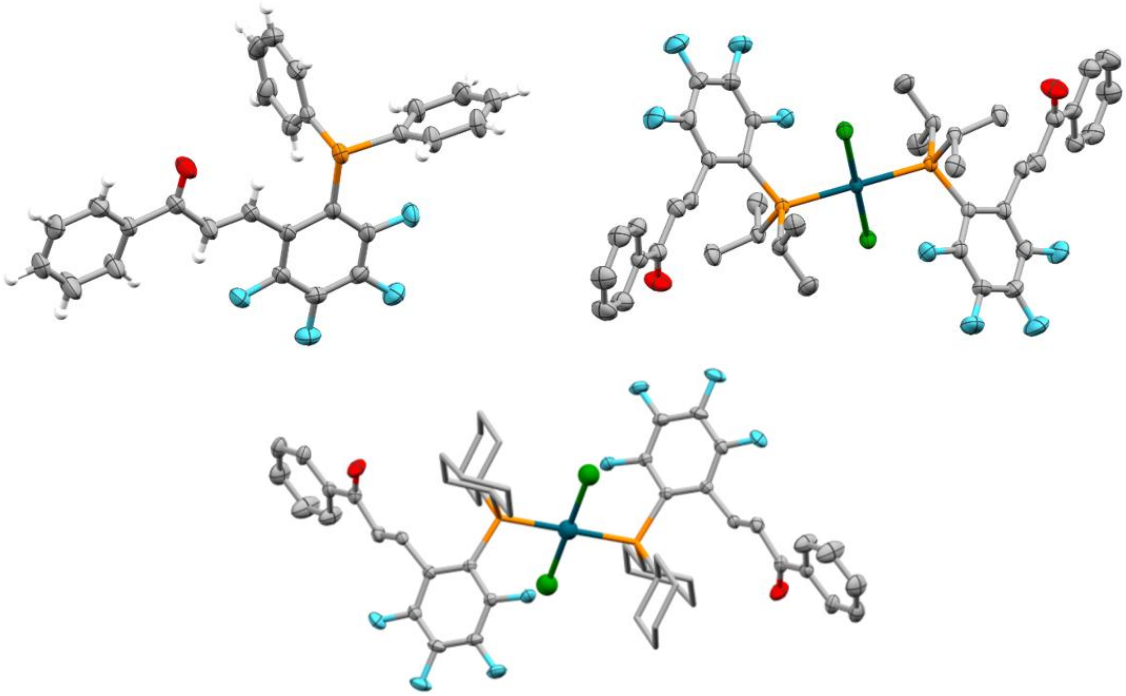

Figure S1. X-ray structures of **L^1** (top, left) and **1L^3** (top, right) and **1L^2** (bottom). H atoms and solvent molecule of **1L^3** and **1L^2** omitted for clarity.

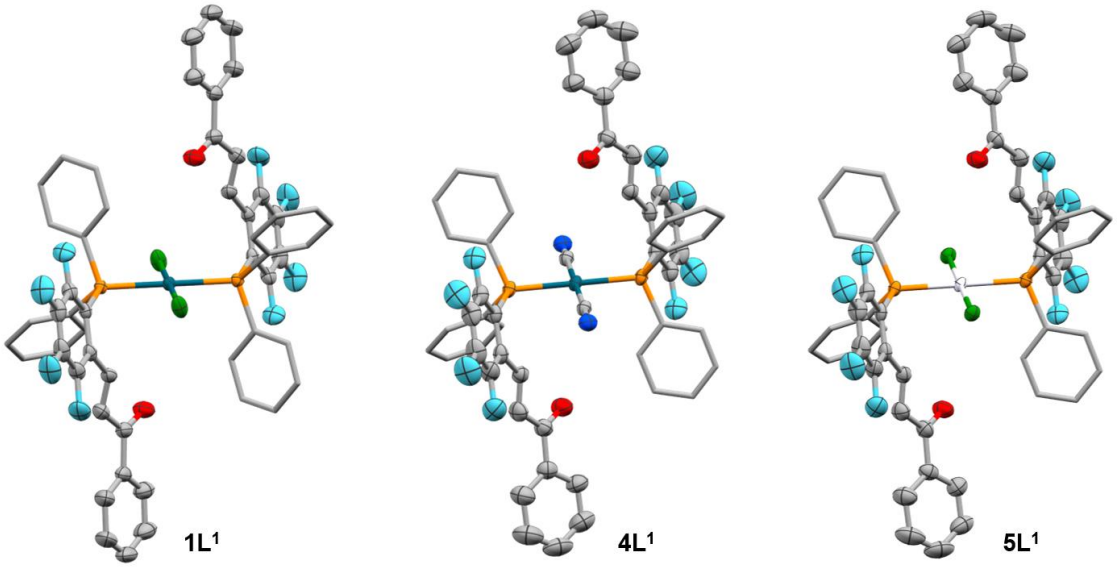

Figure S2. X-ray structures of **1L^1**, **4L^1** and **5L^1**. H atoms omitted for clarity. Relevant distances in Å: **1L^1**: Pd-Cl = 2.2903(7), Pd-P = 2.3231(7), C=C(olefin) = 1.314(4). **4L^1**: Pd-C = 1.990(4), Pd-P = 2.3388(10), C=C(olefin) = 1.320(6). **5L^1**: Pt-Cl = 2.3029(11), Pt-P = 2.3241(11), C=C(olefin) = 1.303(7).

Table S1. Crystal data and structure refinements for compounds **L[1]**, **1L[2]** and **1L[3]**.

Identification code	**L[1]**	[**1L[2]**]·2 acetone	[**1L[3]**]·*n*-hexane
CCDC deposition N°	2205016	2205014	2205013
Empirical formula	$C_{27}H_{17}OF_4P$	$C_{60}H_{70}Cl_2F_8O_4P_2Pd$	$C_{48}H_{56}Cl_2F_8O_2P_2Pd$
Formula weight	464.38	1246.4	1056.16
Temperature/K	294.0	209.9(6)	294.0
Crystal system	monoclinic	triclinic	triclinic
Space group	$P2_1/n$	P-1	P-1
a/Å	12.2385(6)	9.9875(4)	9.5648(5)
b/Å	5.6909(4)	10.2176(3)	11.8739(7)
c/Å	32.1400(16)	15.2240(8)	11.8921(8)
α/°	90	74.659(4)	74.065(5)
β/°	97.755(5)	89.730(4)	70.863(5)
γ/°	90	88.099(3)	78.505(5)
Volume/Å^3	2218.0(2)	1497.39(11)	1218.03(14)
Z	4	1	1
ρ_{calc}g/cm^3	1.391	1.382	1.44
μ/mm^{-1}	0.175	0.522	0.624
F(000)	952	644	542
Crystal size/mm^3	0.527 × 0.098 × 0.049	0.22 × 0.157 × 0.105	0.155 × 0.143 × 0.116
Radiation	MoKα (λ = 0.71073)	MoKα (λ = 0.71073)	MoKα (λ = 0.71073)
2Θ range for data collection/°	6.72 to 49.994	6.904 to 59.51	6.898 to 59.258
Index ranges	-14 ≤ h ≤ 14, -4 ≤ k ≤ 6, -38 ≤ l ≤ 33	-13 ≤ h ≤ 10, -14 ≤ k ≤ 13, -19 ≤ l ≤ 20	-12 ≤ h ≤ 12, -16 ≤ k ≤ 14, -13 ≤ l ≤ 14
Reflections collected	7703	10840	8436
Independent reflections	3878 [R_{int} = 0.0311, R_{sigma} = 0.0503]	6875 [R_{int} = 0.0312, R_{sigma} = 0.0682]	5555 [R_{int} = 0.0282, R_{sigma} = 0.0605]
Data/restraints/parameters	3878/0/298	6875/0/351	5555/2/291
Goodness-of-fit on F^2	1.023	1.034	1.082
Final R indexes [I>=2σ (I)]	R_1 = 0.0529, wR_2 = 0.1042	R_1 = 0.0491, wR_2 = 0.0923	R_1 = 0.0471, wR_2 = 0.0899
Final R indexes [all data]	R_1 = 0.0843, wR_2 = 0.1210	R_1 = 0.0744, wR_2 = 0.1060	R_1 = 0.0705, wR_2 = 0.1087
Largest diff. peak/hole / e Å^{-3}	0.28/-0.18	0.50/-0.44	0.44/-0.51

Table S2. Crystal data and structure refinements for compounds **4L[1]** and **5L[1]**.

Identification code	**4L[1]**	**5L[1]**
CCDC deposition N°	2205015	2205017
Empirical formula	$C_{56}H_{34}F_8N_2O_2P_2Pd$	$C_{54}H_{34}Cl_2F_8O_2P_2Pt$
Formula weight	1087.19	1194.74
Temperature/K	294.0	294.0
Crystal system	monoclinic	monoclinic
Space group	$P2_1/n$	$P2_1/n$
a/Å	14.2828(10)	13.9677(8)
b/Å	10.9456(9)	10.9580(5)
c/Å	16.2908(9)	16.3180(7)
α/°	90	90
β/°	109.972(7)	109.719(5)
γ/°	90	90
Volume/Å^3	2393.6(3)	2351.1(2)
Z	2	2
ρ_{calc}g/cm^3	1.508	1.688
μ/mm^{-1}	0.532	3.241
F(000)	1096	1176
Crystal size/mm^3	0.496 × 0.207 × 0.039	0.431 × 0.218 × 0.139
Radiation	MoKα (λ = 0.71073)	MoKα (λ = 0.71073)
2Θ range for data collection/°	6.838 to 59.484	6.942 to 59.06
Index ranges	-14 ≤ h ≤ 19, -14 ≤ k ≤ 10, -22 ≤ l ≤ 16	-18 ≤ h ≤ 14, -10 ≤ k ≤ 14, -16 ≤ l ≤ 22
Reflections collected	10247	9845
Independent reflections	5507 [R_{int} = 0.0314, R_{sigma} = 0.0657]	5505 [R_{int} = 0.0312, R_{sigma} = 0.0632]
Data/restraints/parameters	5507/0/322	5505/0/313
Goodness-of-fit on F^2	1.036	1.071
Final R indexes [I>=2σ (I)]	R_1 = 0.0517, wR_2 = 0.1034	R_1 = 0.0390, wR_2 = 0.0645
Final R indexes [all data]	R_1 = 0.1034, wR_2 = 0.1321	R_1 = 0.0751, wR_2 = 0.0789
Largest diff. peak/hole / e Å^{-3}	0.81/-0.60	0.92/-0.61

Photophysical Properties

Figure S3 shows example pictures of samples of $\mathbf{L^1}$ and $\mathbf{1L^1}$ upon irradiation with a bench UV lamp (365 nm). Colour change of the solid is clearly observed, with $\mathbf{1L^1}$ showing a red-shifted emission compared to $\mathbf{L^1}$.

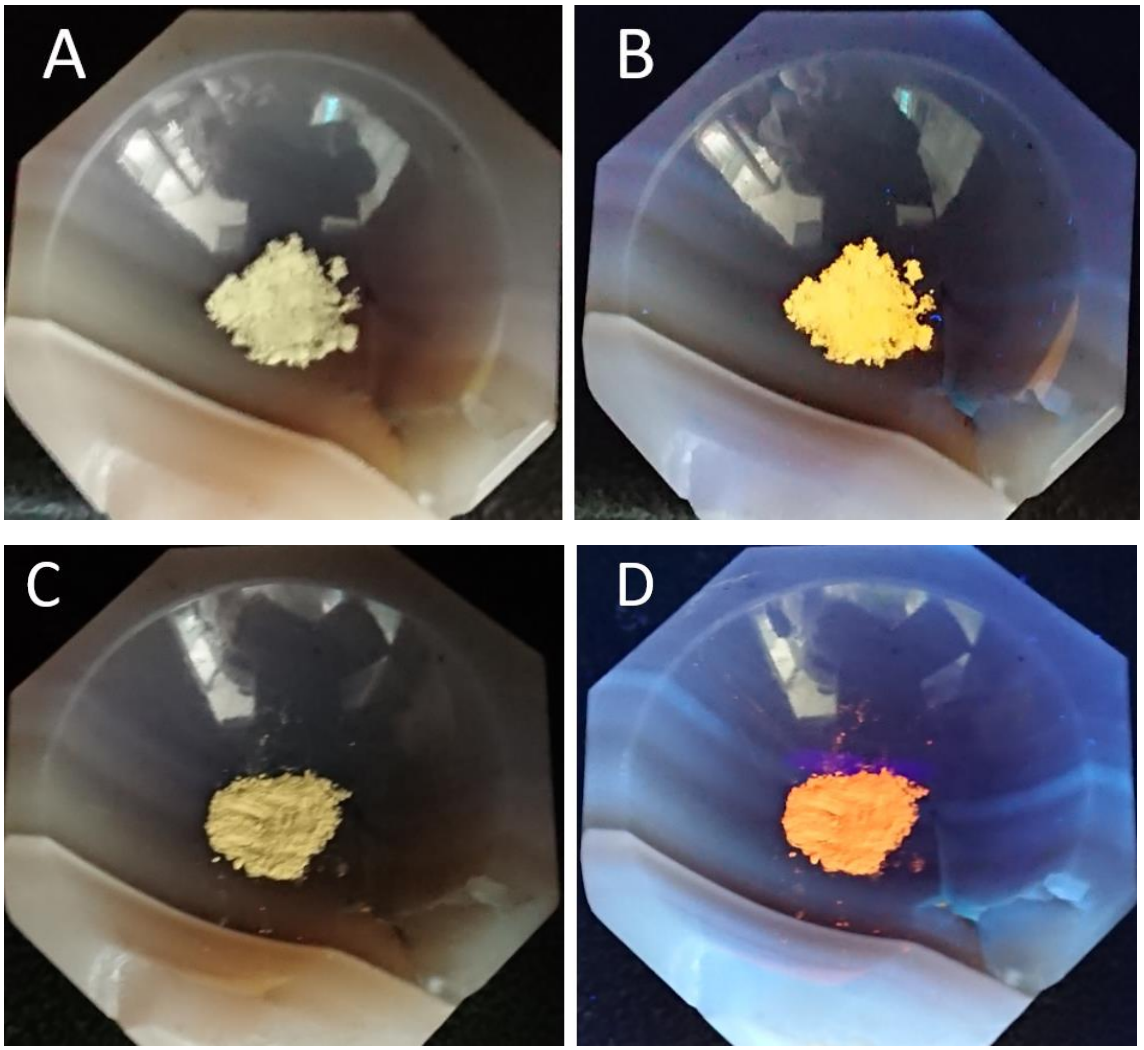

Figure S3. Pictures of $\mathbf{L^1}$ (A, B) and $\mathbf{1L^1}$ (C, D) without (*left*) and with (*right*) irradiation.

Figure S4 and Figure S5 show the normalised emission spectra for ligands and complexes respectively. Representative data of the luminescence properties are gathered in Table S3. Figure S6 - Figure S12 show the emission decay profile of the compounds. Figure S14 and Figure S15 show the normalised excitation spectra for ligands and complexes respectively.

Emission Spectra

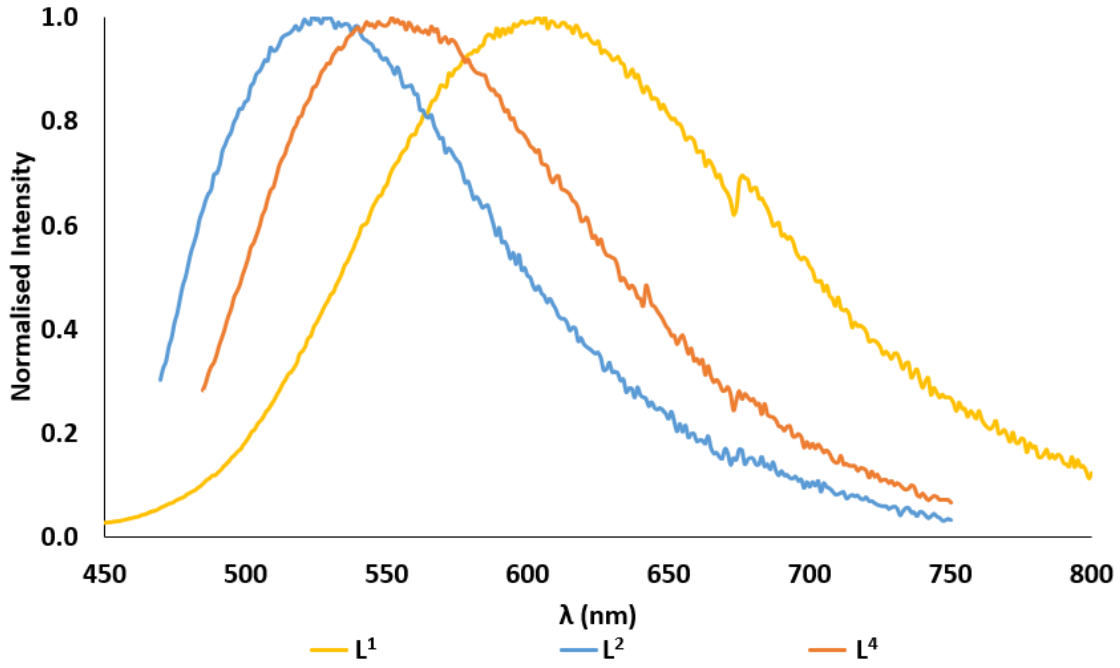

Figure S4. Normalised emission spectra of $\mathbf{L^1}$, $\mathbf{L^2}$ and $\mathbf{L^4}$.

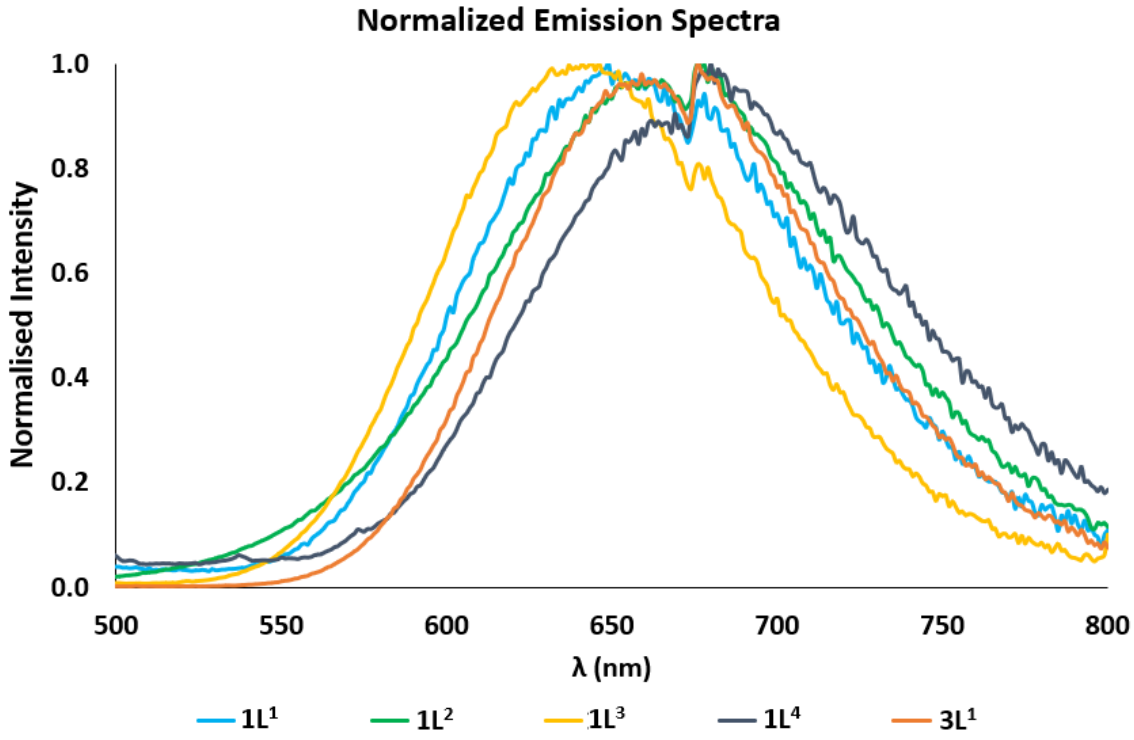

Figure S5. Normalised emission spectra of $\mathbf{1L^1}$, $\mathbf{1L^2}$, $\mathbf{1L^3}$, $\mathbf{1L^4}$ and $\mathbf{3L^1}$.

Luminescence Data

Table S3. Excitation and emission data in the solid state.

Comp	λ_{exc}/nm	λ_{em}/nm	φ/%	τ_{av} [a] /ns	τ_n [b] /ns; A_n [c]
Ph-PEWO-F_4 (L^1)	413	606	10.1	2.47	τ_1 = 1.88; A_1 = 0.51 τ_2 = 6.18; A_2 = 0.49
Cy-PEWO-F_4 (L^2)	460	530	4.1	3.53	τ_1 = 2.23; A_1 = 0.51 τ_2 = 7.20; A_2 = 0.49
Ph-PEWO-H_4 (L^4)	468	552	2.7	3.04	τ_1 = 1.82; A_1 = 0.54 τ_2 = 6.62; A_2 = 0.46
$PdCl_2$(Ph-PEWO-F_4)$_2$ ($1L^1$)	405	649	28.0	1312.49	τ_1 = 152.72; A_1 = 0.06 τ_2 = 1405.88; A_2 = 0.94
$PdCl_2$(Cy-PEWO-F_4)$_2$ ($1L^2$)	412	676	21.8	1623.54	τ_1 = 6.81; A_1 = 0.19 τ_2 = 2005.97; A_2 = 0.81
$PdCl_2$(iPr-PEWO-F_4)$_2$ ($1L^3$)	405	643	15.6	1397.73	τ_1 = 0.97; A_1 = 0.04 τ_2 = 1455.97; A_2 = 0.96
$PdCl_2$(Ph-PEWO-H_4)$_2$ ($1L^4$)	469	680	1.8	637.39	τ_1 = 103.75; A_1 = 0.07 τ_2 = 693.24; A_2 = 0.93
$PdBr_2$(Ph-PEWO-F_4)$_2$ ($3L^1$)	415	666	15.7	5115.10	τ_1 = 508.88; A_1 = 0.12 τ_2 = 5948.2; A_2 = 0.88

[a] Average lifetime: $\tau_{av}= (A_1\tau_1^2+ A_2\tau_2^2+ \cdots) / (A_1\tau_1+ A_2\tau_2+ \cdots)$. [b] Natural lifetime. [c] Intensity coefficients.

Emission Decay Profiles

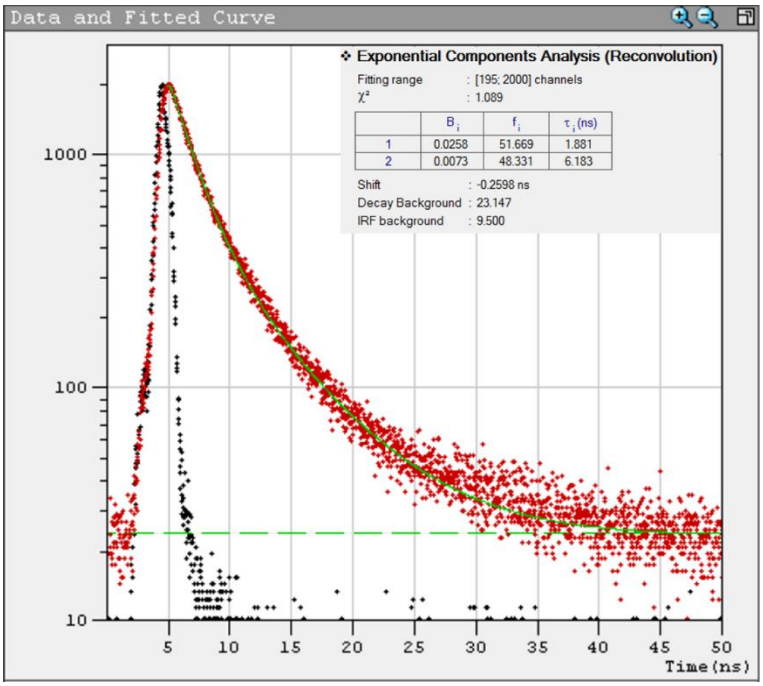

Figure S6. Emission Decay profile of Ph-PEWO-F_4 (**L^1**).

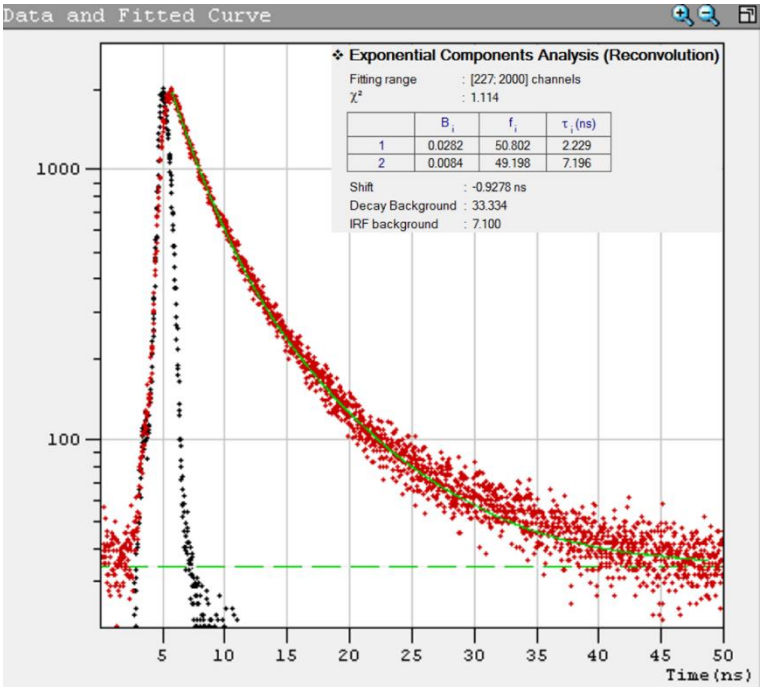

Figure S7. Emission Decay profile of Cy-PEWO-F_4 (**L^2**).

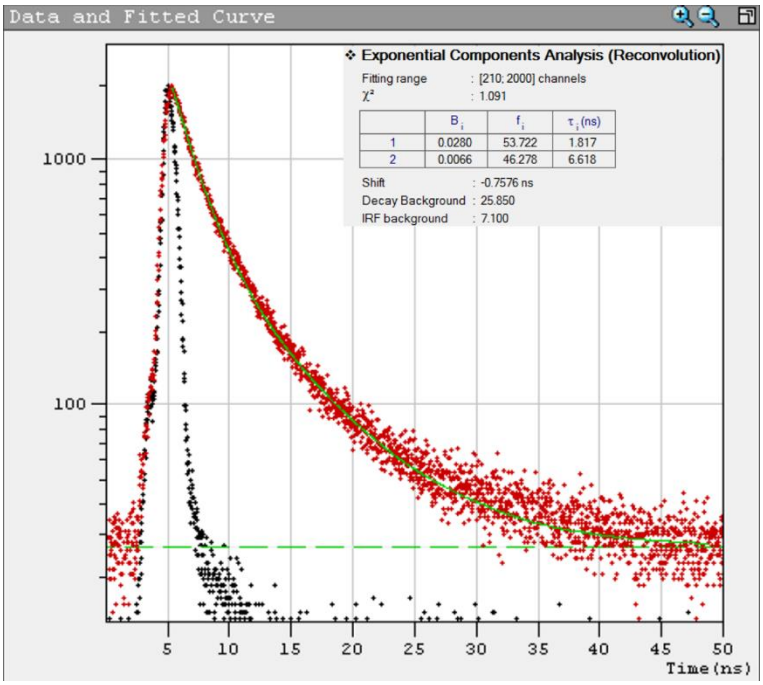

Figure S8. Emission Decay profile of Ph-PEWO-H_4 (**L^4**).

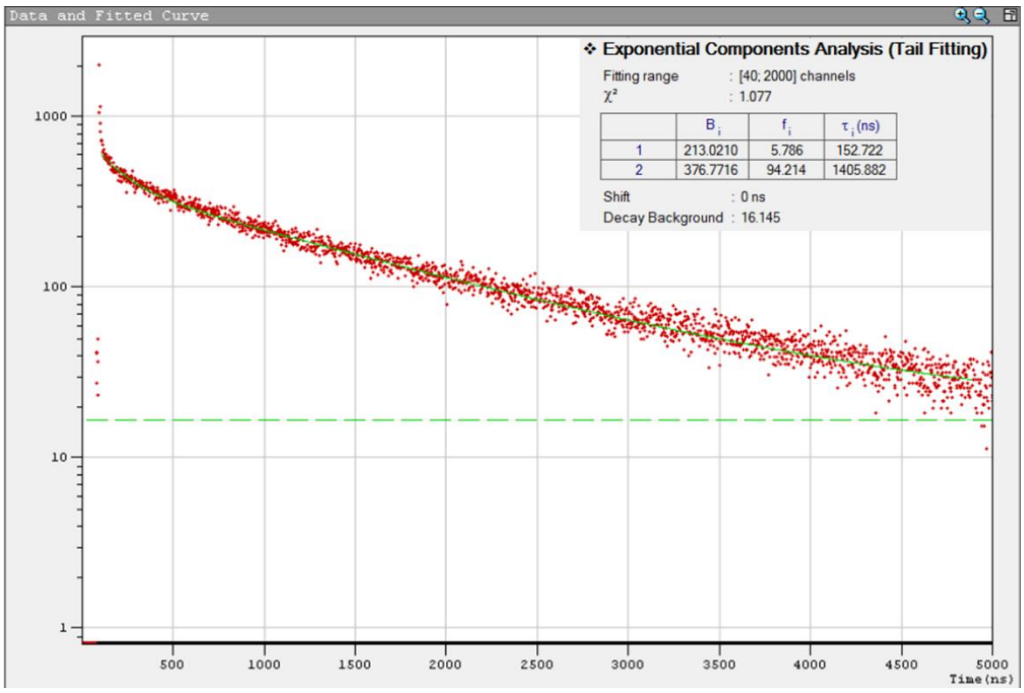

Figure S9. Emission Decay profile of $PdCl_2$(Ph-PEWO-F_4)$_2$ (**$1L^1$**).

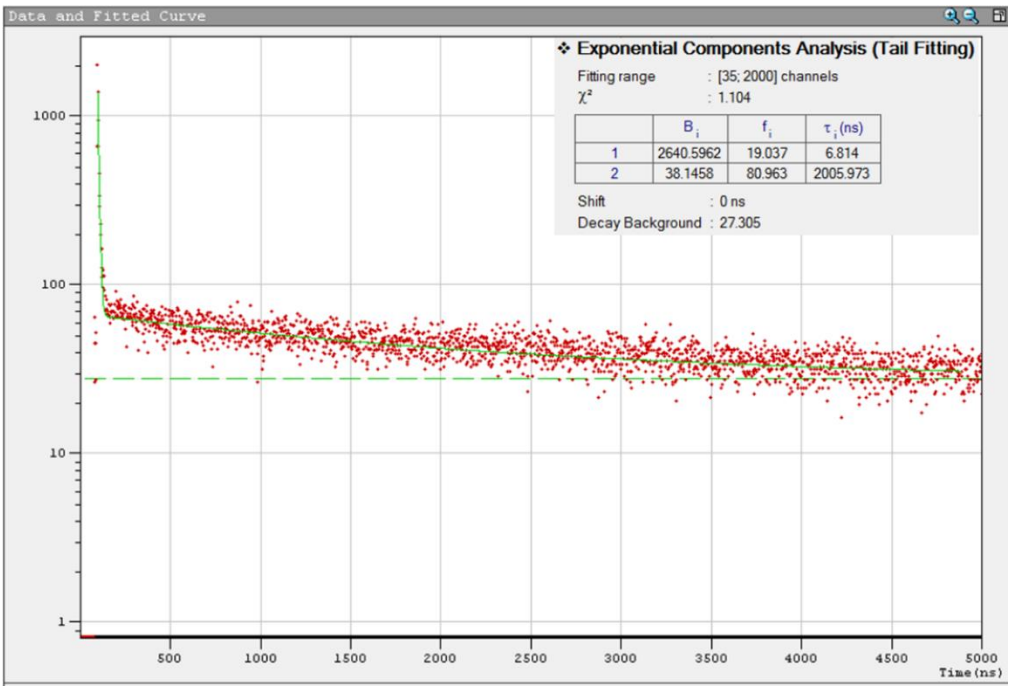

Figure S10. Emission Decay profile of $PdCl_2(Cy\text{-}PEWO\text{-}F_4)_2$ (**1L²**).

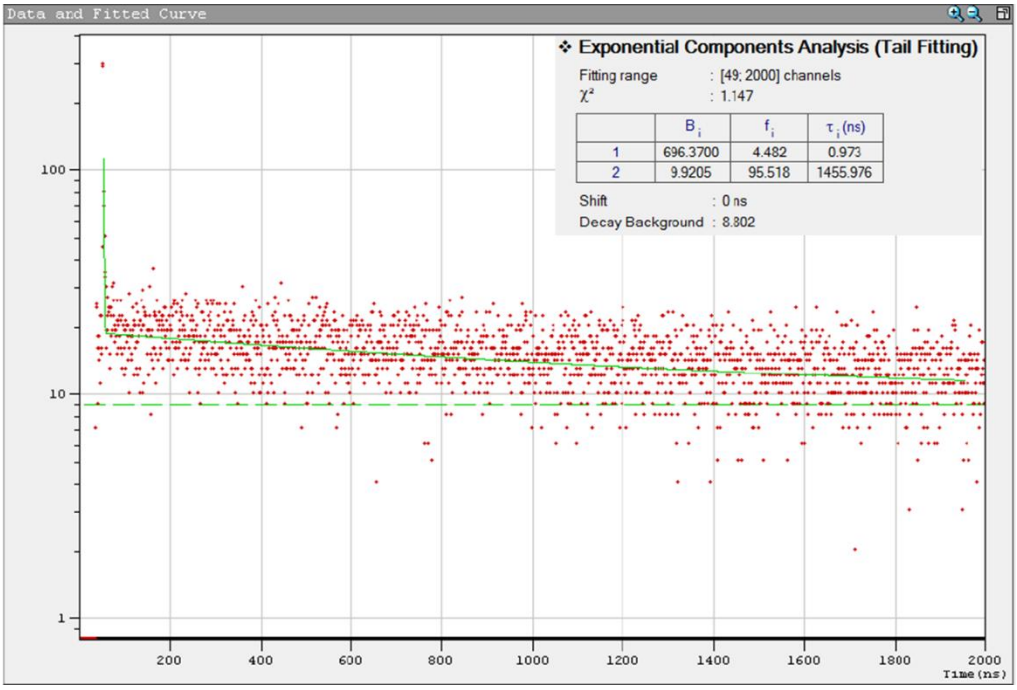

Figure S11. Emission Decay profile of $PdCl_2(iPr\text{-}PEWO\text{-}F_4)_2$ (**1L³**).

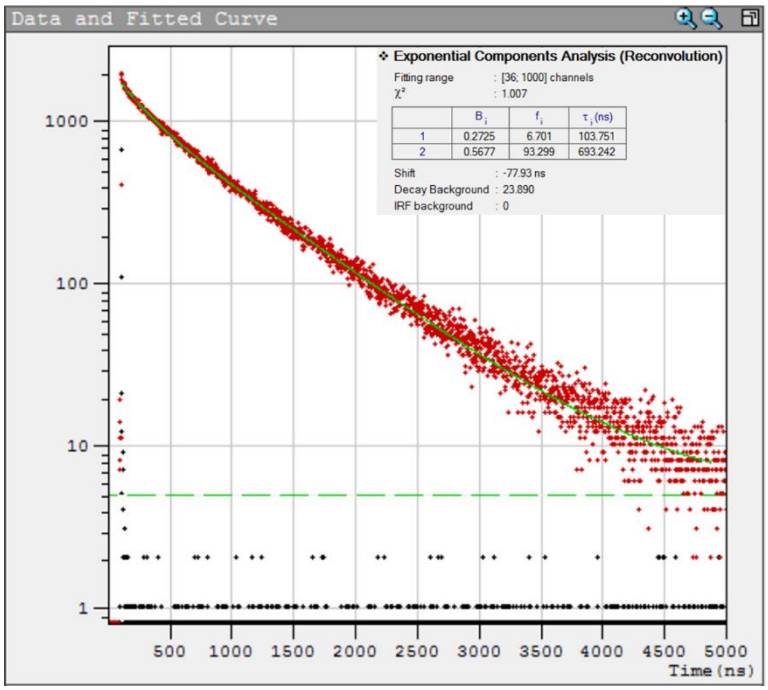

Figure S12. Emission Decay profile of $PdCl_2$(Ph-PEWO-H_4)$_2$ (**1L^4**).

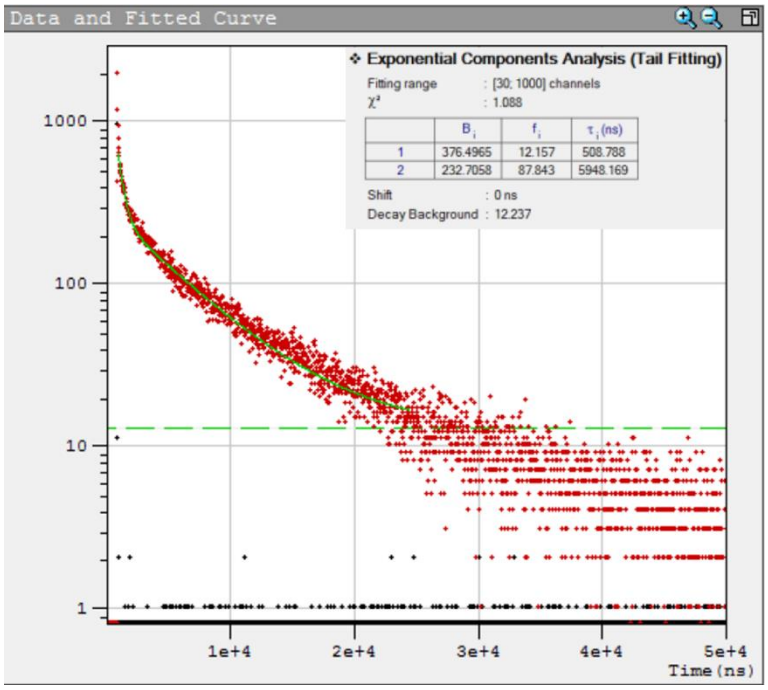

Figure S13. Emission Decay profile of $PdBr_2$(Ph-PEWO-F_4)$_2$ (**3L^1**).

Excitation Spectra

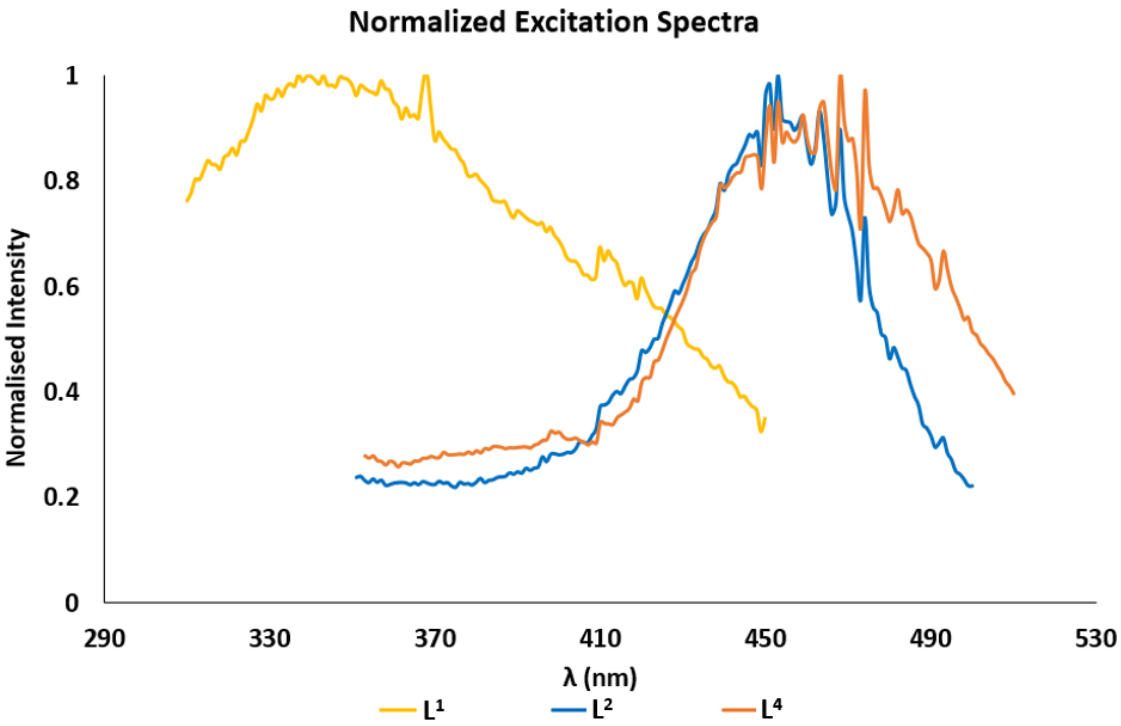

Figure S14. Normalised excitation spectra of $\mathbf{L^1}$, $\mathbf{L^2}$ and $\mathbf{L^4}$.

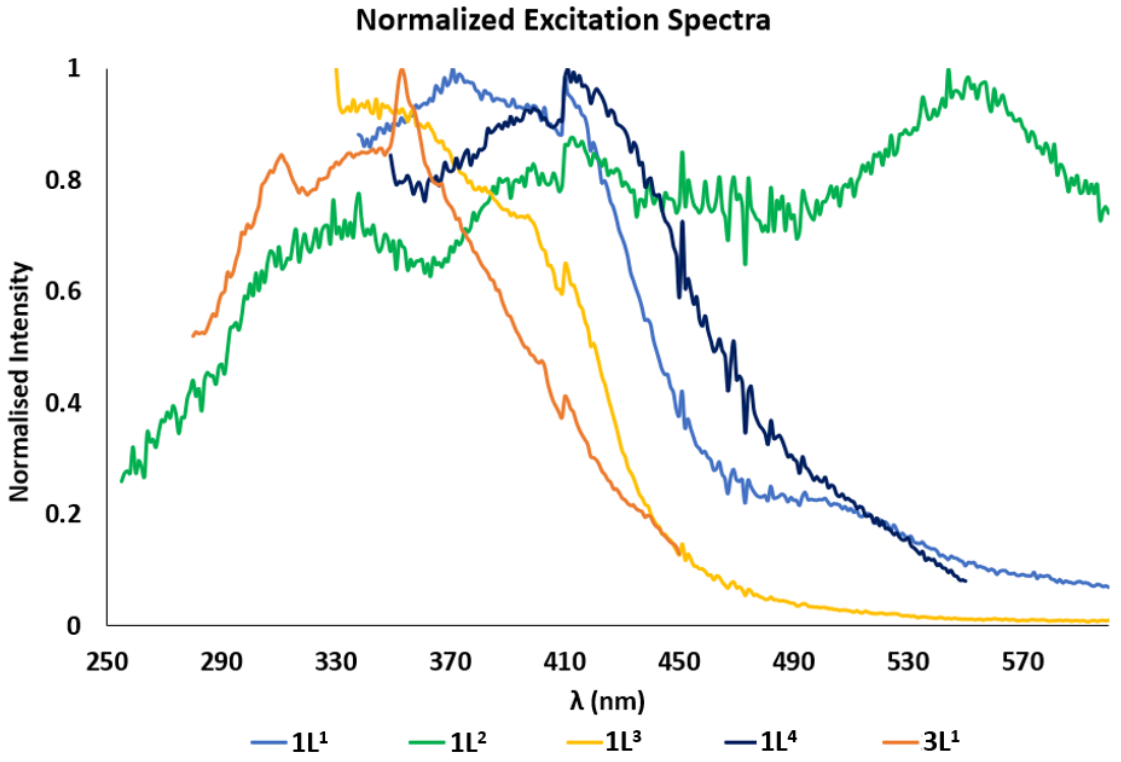

Figure S15. Normalised excitation spectra of $\mathbf{1L^1}$, $\mathbf{1L^2}$, $\mathbf{1L^3}$, $\mathbf{1L^4}$ and $\mathbf{3L^1}$.

DFT Calculations

Computational details

Geometry optimizations in the gas phase were carried out using the Gaussian09 package using the x-ray structures as initial guesses when available.[10] The hybrid density function method known as B3LYP was applied.[11] Effective core potentials (ECP) were used to represent the innermost electrons of the transition atoms (Pd and Pt) and the basis set of valence double-ξ quality for associated with the pseudopotentials known as LANL2DZ.[12] The basis set for the main group elements was 6-31G* (Cl, P, C, N, O, F and H).[13] Excited states and absorption spectra were obtained from the time-depending algorithm implemented in Gaussian09.[14] Acronyms like MLCT or ILCT (metal-ligand or intra-ligand charge transfer respectively) are used in the Tables of this section to categorize the type of electronic transition.

Absorption spectra

Calculated absorption parameters (wavelengths in nm and their intensities) for **L^1** derivatives in the gas phase (Table S4). For metal complexes **1L^1** (Table S5), **5L^1** (Table S6) and **4L^1** (Table S7) only absorptions with intensities *f* factor above 0.10 are shown. For each entry, main contributions of the molecular orbitals for the transition and their coefficients are shown. Moreover, representation of the most relevant molecular orbitals (contour values is fixed to 0.05 e/Å^3) and its composition is added for each compound. Figure S16 shows the simulated absorption spectra for all the compounds studied.

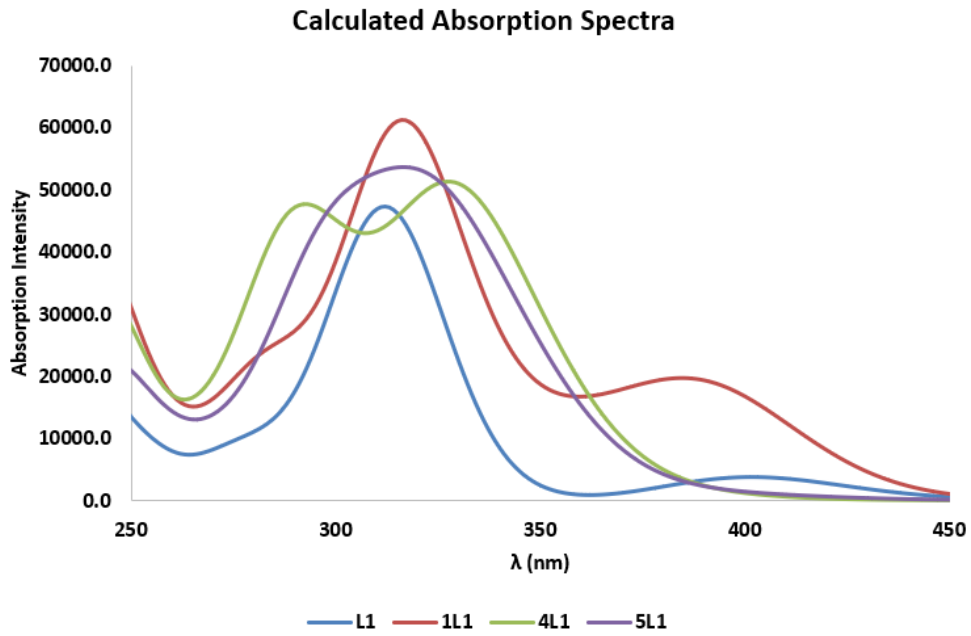

Figure S16. Computed absorption spectra for **L^1** (blue), **1L^1** (red), **4L^1** (green), **5L^1** (purple).

Table S4. Absorption parameters for **L[1]**. The electronic transition coincident with the excitation maximum is highlighted in bold.

λ (*f*)	Assignment	OM
402 (0.05)	**ILCT (PPh_2 → EWO):**	
	$\pi(PPh_2)_{HOMO}$ → $\pi^*(EWO)_{LUMO}$ [88%]	**119 → 120 [0.66]**
314 (0.59)	Chalcone:	
	$\pi(EWO) \rightarrow \pi^*(EWO)_{LUMO}$ [80%]	118 → 120 [0.66]
306 (0.05)	ILCT (PPh_2→ EWO):	
	$\pi(PPh_2) \rightarrow \pi^*(EWO)_{LUMO}$ [73%]	116 → 120 [0.60]
	$\pi(EWO, PPh_2) \rightarrow \pi^*(EWO)_{LUMO}$ [12%]	114 → 120 [0.25]
302 (0.05)	ILCT (PPh_2→ EWO):	
	$\pi (PPh_2)_{HOMO} \rightarrow \pi^*(EWO)$ [45%]	119 → 121 [0.47]
	$\pi (PPh_2) \rightarrow \pi^*(EWO)_{LUMO}$ [22%]	116 → 120 [0.33]
	$\pi (EWO, PPh_2) \rightarrow \pi^*(EWO)_{LUMO}$ [18%]	114 → 120 [0.30]

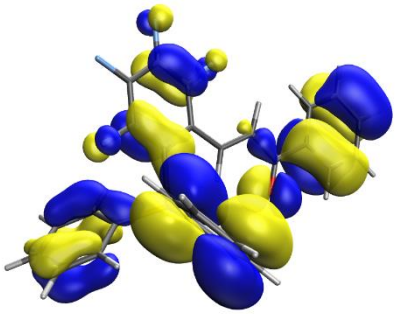

MO 114 (HOMO-3): -0.256 Ha
EWO (58), PPh_2 (42)

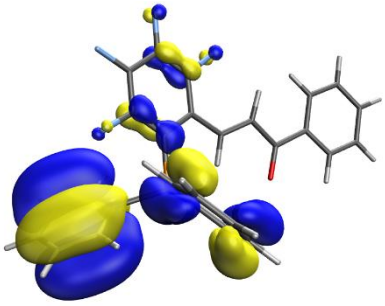

MO 116(HOMO-2): -0.251 Ha
PPh_2 (97)

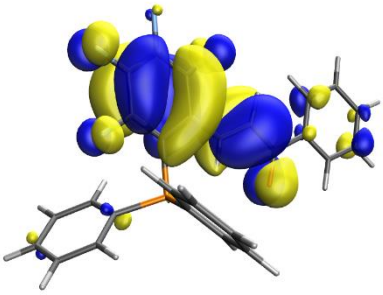

MO 118(HOMO-1): -0.242 Ha
EWO (98)

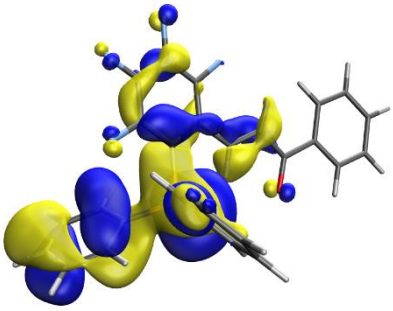

MO 119 (HOMO): -0.221 Ha
PPh_2 (87), EWO (13)

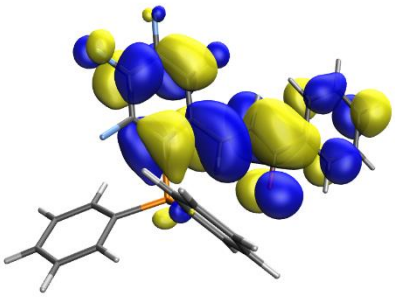

MO 120 (LUMO): -0.085 Ha
EWO (99)

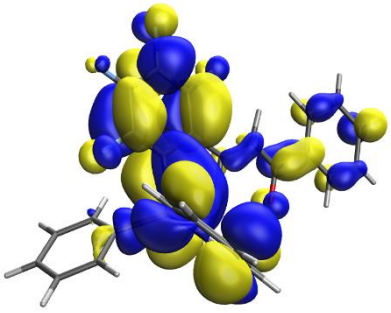

MO 121 (LUMO+1): -0.041 Ha
EWO (67), PPh_2 (33)

Figure S17. Relevant molecular orbitals for **L^1**. Energies and fragment contributions are also shown.

Table S5. Absorption parameters for **1L[1].** The electronic transition coincident with the excitation maximum is highlighted in bold.

λ (*f*)	Assignment	OM
395 (0.20)	**ILCT (PPh_2→ EWO):**	
	π(PPh_2) → π*(EWO),d(Pd)$_{LUMO}$ [77%]	**262 → 265 [0.62]**
318 (0.16)	Chalcone:	
	π(EWO, PPh_2),d(Pd) → π*(EWO) [25%]	259 → 266 [0.35]
	π(EWO),d(Pd) → π*(EWO) [25%]	260 → 266 [0.35]
	π(PPh_2, EWO) → π*(EWO),d(Pd)$_{LUMO}$ [10%]	248 → 265 [0.22]
	π(PPh_2) → π*(EWO) [8%]	258 → 267 [0.20]
317 (0.29)	Chalcone:	
	π(EWO) → π*(EWO),d(Pd)$_{LUMO}$ [20%]	247 → 265 [0.32]
	π(PPh_2, EWO) → π*(EWO),d(Pd)$_{LUMO}$ [19%]	248 → 265 [0.31]
	π(EWO, PPh_2),d(Pd) → π*(EWO) [13%]	259 → 266 [0.26]
	π(EWO),d(Pd) → π*(EWO) [12%]	260 → 266 [0.24]
	lp(Cl),π(PPh_2) → π*(EWO),d(Pd)$_{LUMO}$ [11%]	244 → 265 [0.24]
315 (0.25)	Chalcone:	
	π(EWO) → π*(EWO) [47%]	261 → 267 [0.48]
	π(PPh_2, EWO) → π*(EWO),d(Pd)$_{LUMO}$ [24%]	248 → 265 [0.35]

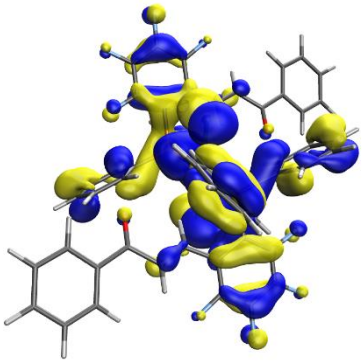

MO 262 (HOMO-2): -0.236 Ha
PPh_2 (29+29), $PdCl_2$ (22) [Cl (9+9)], EWO (10+10)

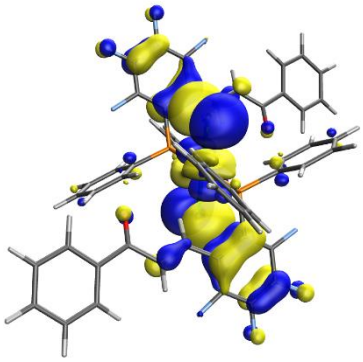

MO 263 (HOMO-1): -0.234 Ha
$PdCl_2$ (77) [Cl (31+31)], EWO (9+9)

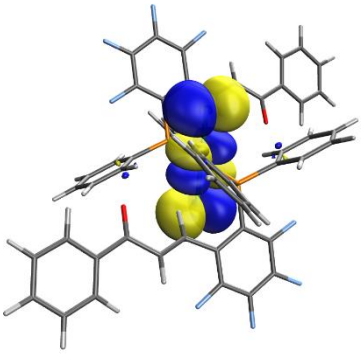

MO 264 (HOMO): -0.227 Ha
$PdCl_2$ (97) [Pd (33)]

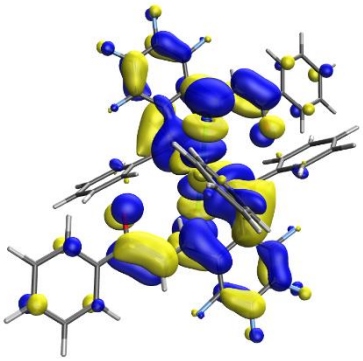

MO 265 (LUMO): -0.096 Ha
$PdCl_2$ (41) [Pd (24)], EWO (19+19), PPh_2 (10+10)

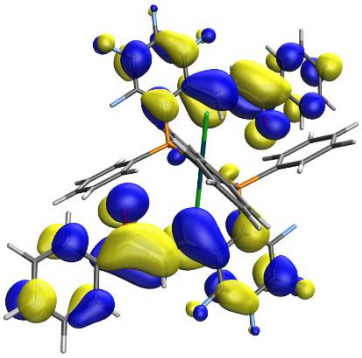

MO 266 (LUMO+1): -0.085 Ha
EWO (48+48)

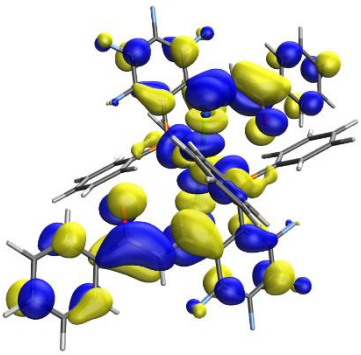

MO 267 (LUMO+2): -0.080 Ha
EWO (33+33), $PdCl_2$ (22), PPh_2 (6+6)

Figure S18. Relevant molecular orbitals for **1L[1]** (from HOMO-2 to LUMO+2). Energies and fragment contributions are also shown.

Table S6. Absorption parameters for **5L[1]**.

λ (*f*)	Assignment	OM
349 (0.16)	Chalcone:	
	$\pi(PPh_2, EWO) \rightarrow \pi^*(EWO)_{LUMO}$ [71%]	262 → 265 [0.60]
	$\pi(EWO) \rightarrow \pi^*(EWO)_{LUMO}$ [17%]	260 → 265 [0.29]
333 (0.18)	Chalcone:	
	$\pi(EWO) \rightarrow \pi^*(EWO)_{LUMO}$ [60%]	260 → 265 [0.55]
	$\pi(PPh_2, EWO) \rightarrow \pi^*(EWO)_{LUMO}$ [15%]	262 → 265 [0.27]
	$\pi(PPh_2) \rightarrow \pi^*(EWO)_{LUMO}$ [10%]	258 → 265 [0.22]
324 (0.26)	ILCT (PPh_2→ EWO):	
	$\pi(PPh_2) \rightarrow \pi^*(EWO)_{LUMO}$ [70%]	258 → 265 [0.59]
	$\pi(EWO) \rightarrow \pi^*(EWO)_{LUMO}$ [11%]	260 → 265 [0.24]
317 (0.17)	Chalcone:	
	$\pi(EWO) \rightarrow \pi^*(EWO)$ [79%]	259 → 266 [0.63]
303 (0.14)	LMCT (PPh_2→ Pt):	
	$\pi(PPh_2, EWO) \rightarrow d(Pt)$ [36%]	262 → 267 [0.42]
	$\pi(EWO) \rightarrow d(Pt)$ [28%]	260 → 267 [0.37]
296 (0.14)	LMCT (EWO → Pt):	
	$\pi(PPh_2, EWO) \rightarrow d(Pt)$ [35%]	262 → 267 [0.42]
	$\pi(EWO) \rightarrow d(Pt)$ [13%]	260 → 267 [0.26]

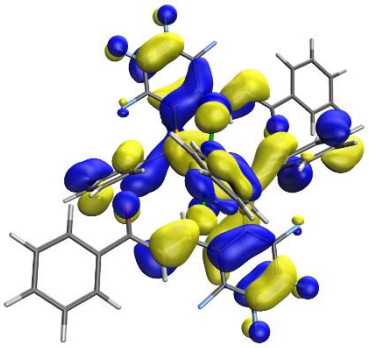

MO 262 (HOMO-2): -0.239 Ha
PPh_2 (25+25), **EWO (22+22)**, $PtCl_2$ (7)

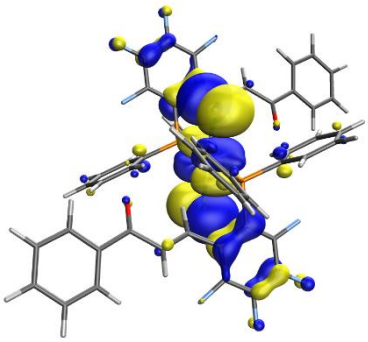

MO 263 (HOMO-1): -0.231 Ha
$PtCl_2$ (85) [Cl (32+32)], EWO (5+5)

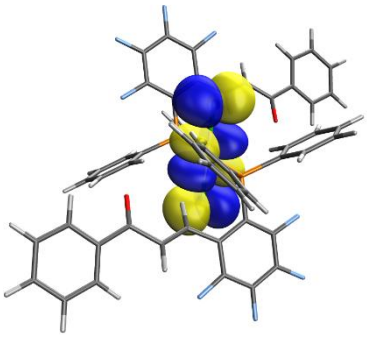

MO 264 (HOMO): -0.218 Ha
$PtCl_2$ (98) [Pt (44)]

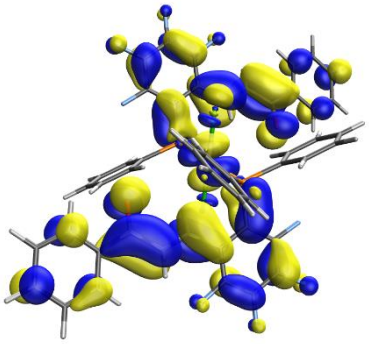

MO 265 (LUMO): -0.088 Ha
EWO (43+43), $PtCl_2$ (7), PPh_2 (3+3)

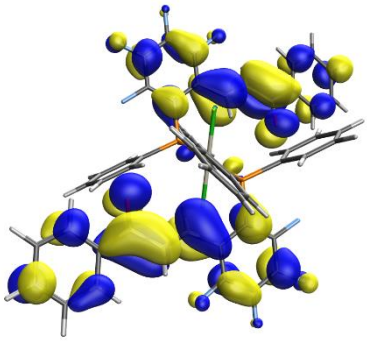

MO 266 (LUMO+1): -0.085 Ha
EWO (48+48)

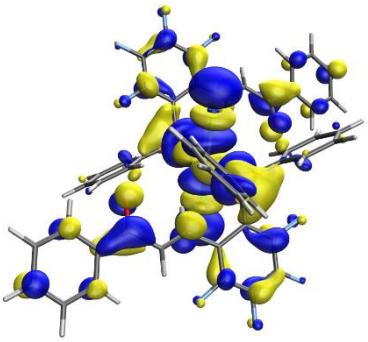

MO 267 (LUMO+2): -0.065 Ha
$PtCl_2$ (51) [Pt (28)], EWO (12+12), PPh_2 (12+12)

Figure S19. Molecular orbitals for **5L[1]** (from HOMO-2 to LUMO+2). Energies and fragment contributions are also shown.

Table S7. Absorption parameters for **4L[1]**.

λ (*f*)	Assignment	OM
350 (0.19)	Chalcone:	
	$\pi(EWO,PPh_2)_{HOMO} \rightarrow \pi^*(EWO)_{LUMO}$ [77%]	260 → 261 [0.62]
	$\pi(EWO) \rightarrow \pi^*(EWO)_{LUMO}$ [17%]	258 → 261 [0.29]
333 (0.32)	Chalcone:	
	$\pi(EWO) \rightarrow \pi^*(EWO)_{LUMO}$ [71%]	258 → 261 [0.60]
	$\pi(EWO, PPh_2)_{HOMO} \rightarrow \pi^*(EWO)_{LUMO}$ [17%]	260 → 261 [0.29]
325 (0.16)	ILCT (PPh_2→ EWO):	
	$\pi(PPh_2)$,d(Pd) → π*(EWO) [49%]	257 → 262 [0.50]
	π(EWO) → π*(EWO) [23%]	259 → 262 [0.34]
322 (0.12)	Chalcone:	
	π(EWO) → π*(EWO) [42%]	259 → 262 [0.46]
	$\pi(PPh_2)$,d(Pd) → π*(EWO) [38%]	257 → 262 [0.44]
	$\pi(PPh_2) \rightarrow \pi^*(EWO)_{LUMO}$ [9%]	256 → 261 [0.21]
298 (0.12)	ILCT (Phos → EWO):	
	$\pi(PPh_2) \rightarrow \pi^*(EWO)_{LUMO}$ [35%]	243 → 261 [0.42]
	$\pi(EWO) \rightarrow \pi^*(EWO)_{LUMO}$ [20%]	245 → 261 [0.31]
	$\pi(PPh_2)$,d(Pd) → π*(EWO) [16%]	242 → 262 [0.28]
	$\pi(PPh_2$,EWO,CN) → π*(EWO) [9%]	252 → 262 [0.21]
	π(EWO) → π*(EWO) [8%]	244 → 262 [0.20]
293 (0.11)	Chalcone:	
	$\pi(PPh_2) \rightarrow \pi^*(EWO)_{LUMO}$ [22%]	243 → 261 [0.33]
	$\pi(EWO) \rightarrow \pi^*(EWO)_{LUMO}$ [18%]	245 → 261 [0.30]
	$\pi(EWO, PPh_2)_{HOMO} \rightarrow$ π*(EWO),d(Pd) [17%]	260 → 263 [0.29]
	π(EWO) → π*(EWO) [10%]	244 → 262 [0.23]
288 (0.30)	Chalcone:	
	$\pi(EWO, PPh_2)_{HOMO} \rightarrow$ π*(EWO),d(Pd) [52%]	260 → 263 [0.51]
	$\pi(PPh_2) \rightarrow \pi^*(EWO)_{LUMO}$ [13%]	243 → 261 [0.26]

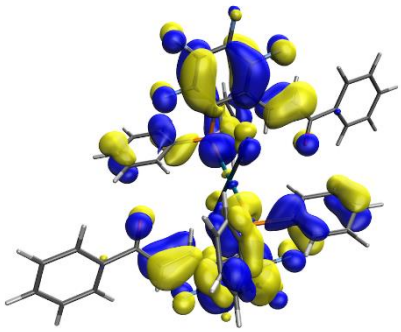

MO 258 (HOMO-2): -0.244 Ha
EWO (33+33), PPh_2 (15+15)

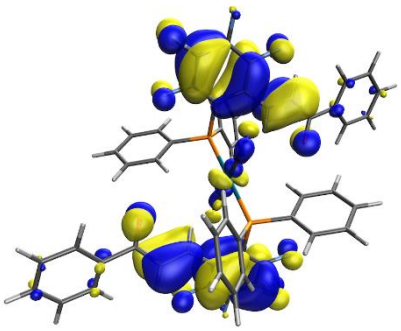

MO 259 (HOMO-1): -0.243 Ha
EWO (48+48)

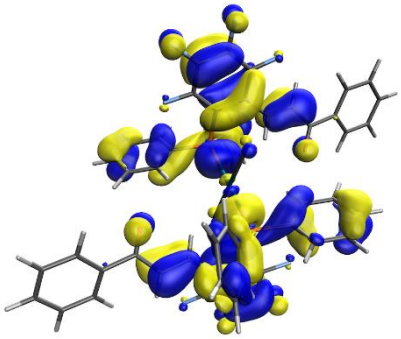

MO 260 (HOMO): -0.241 Ha
EWO (28+28), **PPh_2 (20+20)**

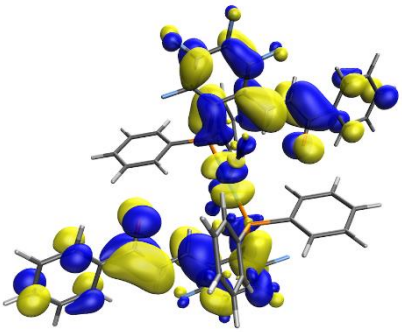

MO 261 (LUMO): -0.092 Ha
EWO (43+43), $Pd(CN)_2$ (8)

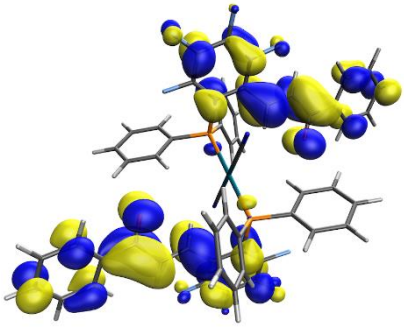

MO 262 (LUMO+1): -0.089 Ha
EWO (48+48)

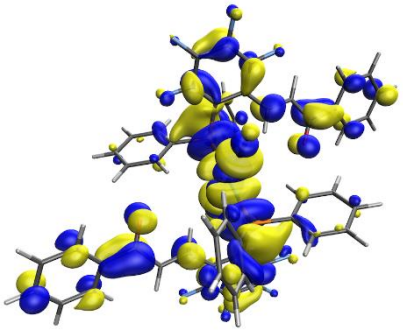

MO 263 (LUMO+2): -0.065 Ha
$Pd(CN)_2$ (40) [Pd (26)], EWO (16+16), PPh_2 (15+15)

Figure S20. Molecular orbitals for **4L[1]** (from HOMO-2 to LUMO+2). Energies and fragment contributions are also shown.

Phosphorescence emission

Calculated triplet states (wavelengths in nm) for the **L[1]** derivatives in ground state, together with their main monoexcitations. For each entry, main contributions of the molecular orbitals involved in the transition and their coefficients are shown.

Table S8. Potentially phosphorescent emissions computed for **L[1]**. Note that neither of those fit with the experimental emission with maximum around 600 nm.

T_n	Assignment	OM
515 (T_1)	Chalcone:	
	π(EWO) → π^*(EWO)$_{LUMO}$ [74%]	118 → 120 [0.61]
	π(PPh$_2$)$_{HOMO}$ → π^*(EWO) [10%]	119 → 120 [0.22]
456 (T_2)	Chalcone:	
	π(EWO) → π^*(EWO)$_{LUMO}$ [85%]	117 → 120 [0.65]
410 (T_3)	ILCT (PPh$_2$→ EWO):	
	π(PPh$_2$)$_{HOMO}$ → π^*(EWO) [82%]	119 → 120 [0.64]
	π(EWO) → π^*(EWO)$_{LUMO}$ [10%]	118 → 120 [0.33]

* Reoptimizing T_1

λ_{Ph}	Assignment	OM
512	Chalcone:	
	π(EWO) ← π^*(EWO) [90%]	115 ← 120 [0.67]
	π(PPh$_2$) ← π^*(EWO) [4%]	116 ← 120 [0.21]

Table S9. Potentially phosphorescent emissions computed for **1L[1]**. The electronic transition coincident with the emission maximum is highlighted in bold.

T_n	Assignment	OM
667 (T_1)	**MLCT (Pd → EWO):**	
	d(Pd) → π*(EWO),d(Pd)$_{LUMO}$ [71%]	**264 → 265 [0.60]**
	d(Pd) → π*(EWO) [20%]	**264 → 267 [0.32]**
575 (T_2)	Chalcone:	
	π(EWO),d(Pd) → π*(EWO),d(Pd)$_{LUMO}$ [25%]	260 → 265 [0.35]
	π(EWO, PPh_2),d(Pd) → π*(EWO),d(Pd)$_{LUMO}$ [22%]	259 → 265 [0.34]
		252 → 265 [0.24]
	π(PPh_2),d(Pd) → π*(EWO),d(Pd)$_{LUMO}$ [12%]	
547 (T_3)	LLCT (Cl → EWO):	
	lp(Cl) → π*(EWO),d(Pd)$_{LUMO}$ [65%]	263 → 265 [0.57]
	lp(Cl) → π*(EWO) [14%]	263 → 267 [0.26]
507 (T_4)	Chalcone:	
	π(EWO) → π*(EWO),d(Pd)$_{LUMO}$ [21%]	261 → 265 [0.32]
	π(EWO),d(Pd) → π*(EWO) [15%]	260 → 266 [0.27]
	π(EWO) → π*(EWO) [15%]	261 → 267 [0.27]
	π(EWO, PPh_2),d(Pd) → π*(EWO) [14%]	259 → 266 [0.26]
505 (T_5)	Chalcone:	
	π(EWO) → π*(EWO) [31%]	261 → 266 [0.40]
	π(EWO),d(Pd) → π*(EWO),d(Pd)$_{LUMO}$ [12%]	260 → 265 [0.24]
	π(EWO, PPh_2),d(Pd) → π*(EWO),d(Pd)$_{LUMO}$ [10%]	259 → 265 [0.22]

* Reoptimization of T_1 led to profound structural change, presumably not accesible in the crystalline structure.

Table S10. Potentially phosphorescent emissions computed for **5L[1]**. Note that no sign of luminescence is observed for this compound.

T_n	Assignment	OM
555 (T_1)	MLCT (Pt → EWO):	
	d(Pt) → π*(EWO)$_{LUMO}$ [62%]	264 → 265 [0.56]
	d(Pt) → π*(EWO) [39%]	264 → 267 [0.38]
505 (T_2)	Chalcone:	
	π(EWO) → π*(EWO) [32%]	259 → 266 [0.40]
	π(EWO) → π*(EWO)$_{LUMO}$ [21%]	260 → 265 [0.32]
	π(PPh_2,EWO) → π*(EWO)$_{LUMO}$ [17%]	262 → 265 [0.30]
505 (T_3)	Chalcone:	
	π(EWO) → π*(EWO)$_{LUMO}$ [33%]	259 → 265 [0.41]
	π(EWO) → π*(EWO) [20%]	260 → 266 [0.32]
	π(PPh_2,EWO) → π*(EWO) [16%]	262 → 266 [0.28]

Table S11. Potentially phosphorescent emissions computed for **4L[1]**. Note that no sign of luminescence is observed for this compound. Remarkably, no involvement of palladium orbitals is predicted.

T_n	Assignment	OM
510 (T_1)	Chalcone:	
	π(EWO) → π*(EWO) [37%]	259 → 262 [0.43]
	π(EWO, PPh_2)$_{HOMO}$ → π*(EWO)$_{LUMO}$ [23%]	260 → 261 [0.34]
	π(EWO) → π*(EWO)$_{LUMO}$ [18%]	258 → 261 [0.30]
510 (T_2)	Chalcone:	
	π(EWO) → π*(EWO)$_{LUMO}$ [39%]	259 → 261 [0.44]
	π(EWO, PPh_2)$_{HOMO}$ → π*(EWO) [21%]	260 → 262 [0.32]
	π(EWO) → π*(EWO) [18%]	258 → 262 [0.30]
444 (T_3)	Chalcone:	
	π(EWO) → π*(EWO) [34%]	253 → 262 [0.41]
	π(EWO) → π*(EWO)$_{LUMO}$ [33%]	254 → 261 [0.40]
444 (T_4)	Chalcone:	
	π(EWO) → π*(EWO) [34%]	254 → 262 [0.41]
	π(EWO) → π*(EWO)$_{LUMO}$ [33%]	253 → 261 [0.40]

Fluorescence emission

Calculated fluorescence emission (wavelengths in nm) for the **L^1** derivatives in the first excited singlet state, together their main monoexcitations. For each entry, main contributions of the molecular orbitals involved in the transition and their coefficients are shown.

Table S12. Potentially fluorescent emissions computed for **L^1.** Note that since the two first singlets are centred in perfluorinated chalcone framework, an expected deexcitation would promote the fluorescence emission at 580 nm, that satisfactorily reproduce the experimental emission (short lifetime support fluorescent behaviour).

λ_{FI}	Assignment	OM
580	**Chalcone:**	
	π(EWO) ← π*(EWO) [59%]	**119 ← 120 [0.54]**
	π(PPh_2) ← π*(EWO) [28%]	**118 ← 120 [0.37]**
	π(EWO) ← π*(EWO) [13%]	**117 ← 120 [0.25]**
572	Chalcone:	
	π(EWO) ← π*(EWO) [84%]	117 ← 120 [0.65]
	π(EWO) ← π*(EWO) [11%]	119 ← 120 [0.24]
460	ILCT (PPh_2← EWO):	
	π(PPh_2) ← π*(EWO) [69%]	118 ← 120 [0.59]
	π(EWO) ← π*(EWO) [31%]	119 ← 120 [0.40]

Table S13. Potentially fluorescent emissions computed for **1L[1]**. Note that neither of those fit with the experimental emission with maximum around 650 nm.

λ_{FI}	Assignment	OM
896	MLCT (Cl ← Pd):	
	lp(Cl) ← d(Pd) [58%]	263 ← 265 [0.54]
	d(Pd),lp(Cl) ← d(Pd) [38%]	262 ← 265 [0.44]
837	Pd *d*-*d* band:	
	d(Pd),lp(Cl) ← d(Pd) [46%]	262 ← 265 [0.48]
	lp(Cl) ← d(Pd) [27%]	263 ← 265 [0.37]
	lp(Cl) ← d(Pd) [19%]	261 ← 265 [0.31]
784	MLCT (Cl ← Pd):	
	lp(Cl) ← d(Pd) [68%]	261 ← 265 [0.58]
	d(Pd),lp(Cl) ← d(Pd) [8%]	262 ← 265 [0.20]
561	LMCT (Pd ← EWO):	
	d(Pd),lp(Cl) ← π*(EWO) [99%]	264 ← 266 [0.70]
540	MLCT (PPh_2,EWO ← Pd):	
	π(PPh_2) ←d(Pd) [29%]	257 ← 265 [0.38]
	π(EWO) ←d(Pd) [27%]	260 ← 265 [0.37]
512	MLCT (PPh_2,EWO ← Pd):	
	π(EWO) ←d(Pd) [60%]	260 ← 265 [0.55]
	lp(Cl) ←d(Pd) [27%]	258 ← 265 [0.37]
495	MLCT (EWO ← Pd):	
	π(EWO) ←d(Pd) [93%]	259 ← 265 [0.68]

* Since the three first singlets involve palladium *d*-orbitals, an expected deexcitation would promote the fluorescence emission at 561 nm having LMCT character

NMR Spectra

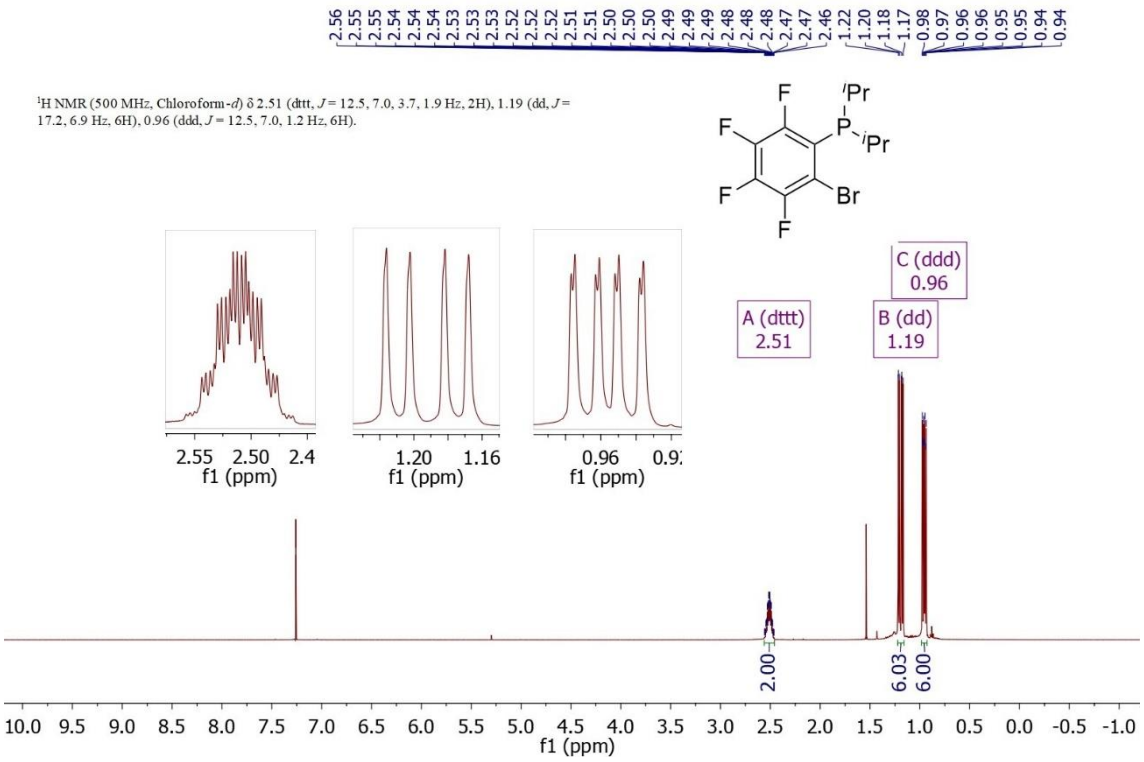

Figure S21. ^{1}H NMR of (2-bromo-3,4,5,6-tetrafluorophenyl)diisopropylphosphine.

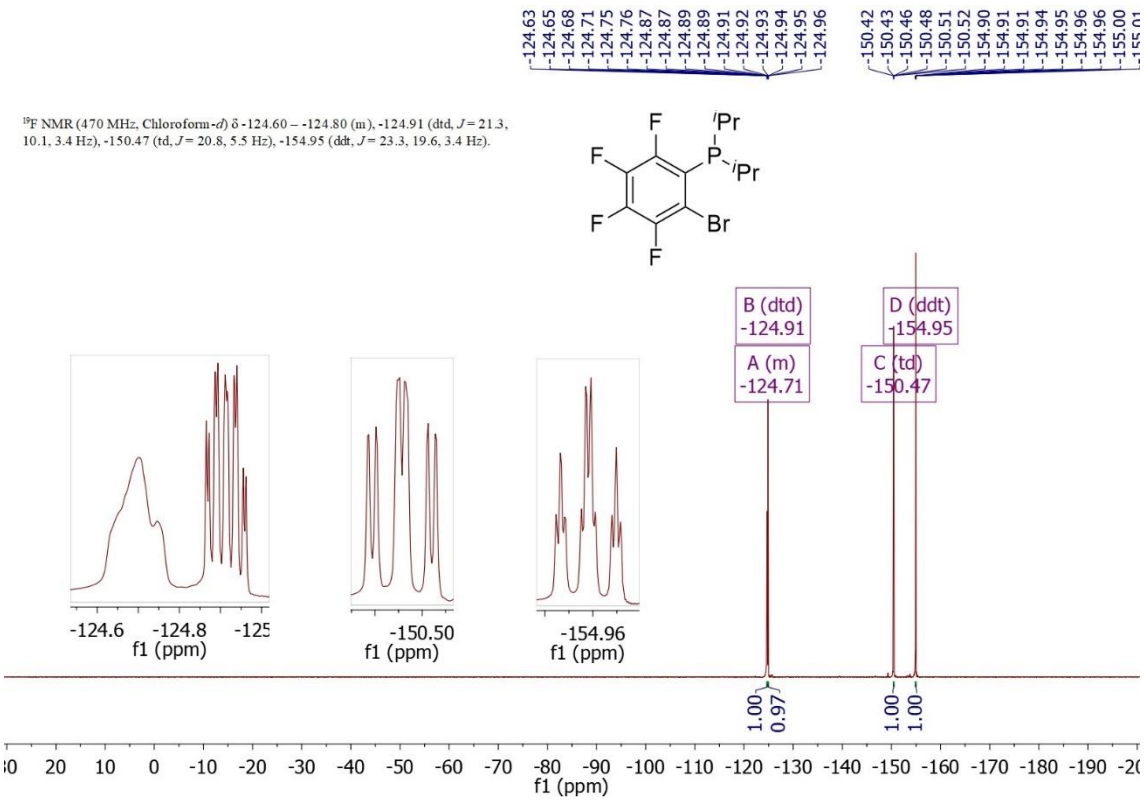

Figure S22. ^{19}F NMR of (2-bromo-3,4,5,6-tetrafluorophenyl)diisopropylphosphine.

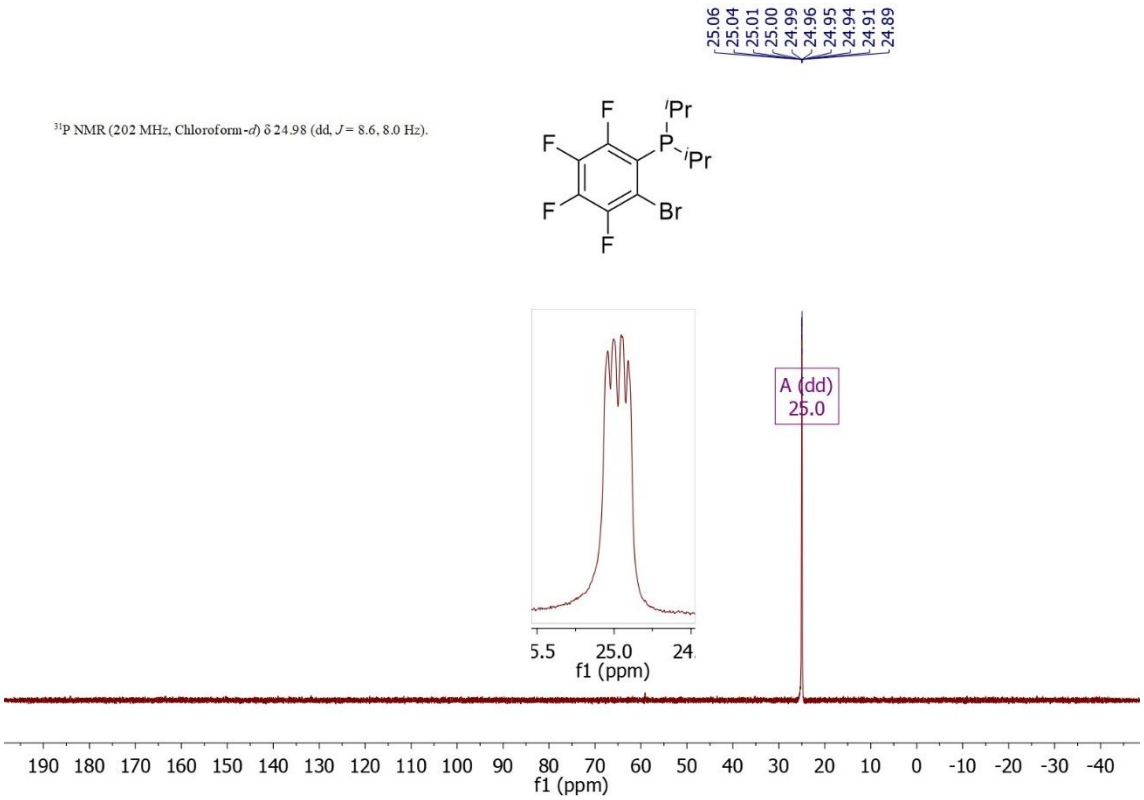

Figure S23. $^{31}P\{^{1}H\}$ NMR of (2-bromo-3,4,5,6-tetrafluorophenyl)diisopropylphosphine.

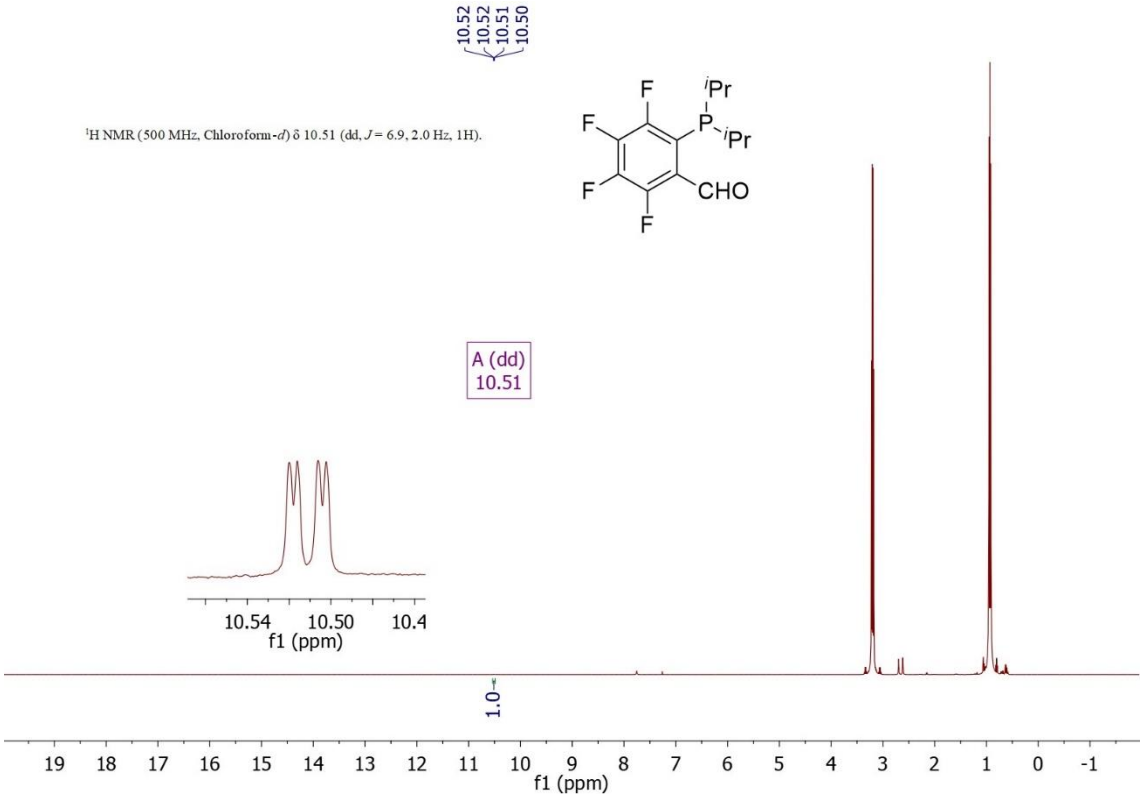

Figure S24. ^{1}H NMR of 2-(diisopropylphosphaneyl)-3,4,5,6-tetrafluorobenzaldehyde.

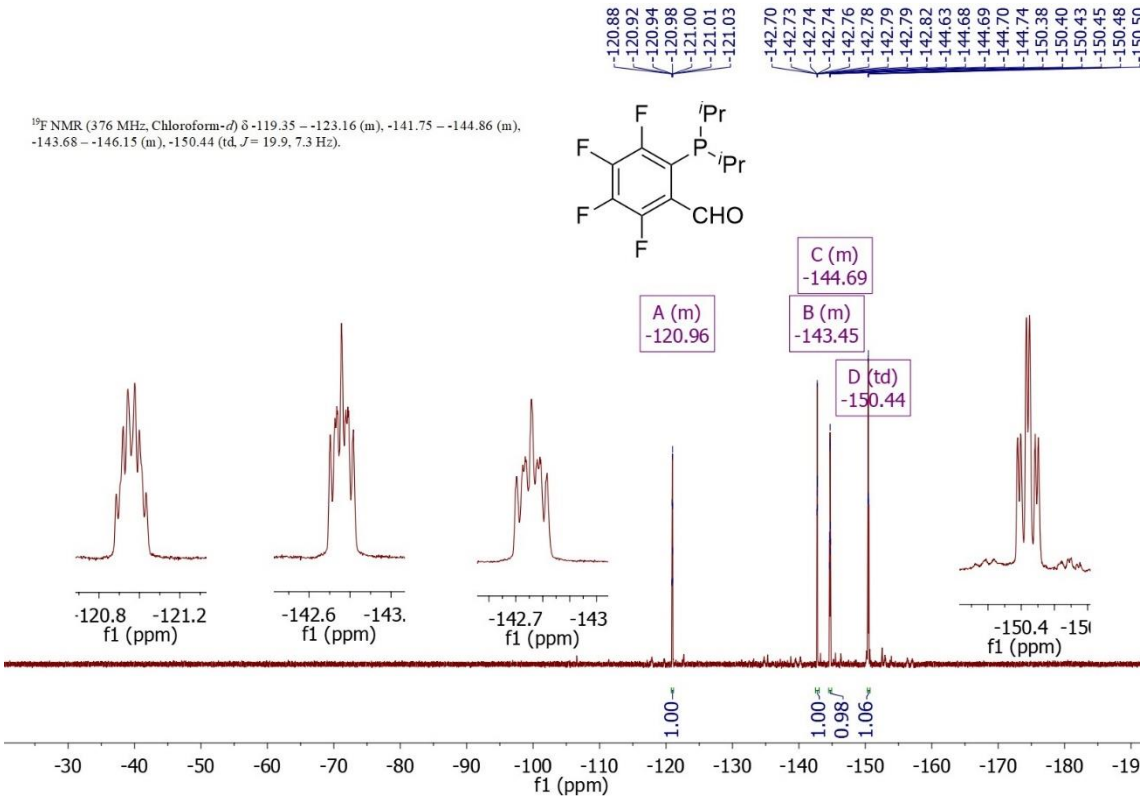

Figure S25. ^{19}F NMR of 2-(diisopropylphosphaneyl)-3,4,5,6-tetrafluorobenzaldehyde.

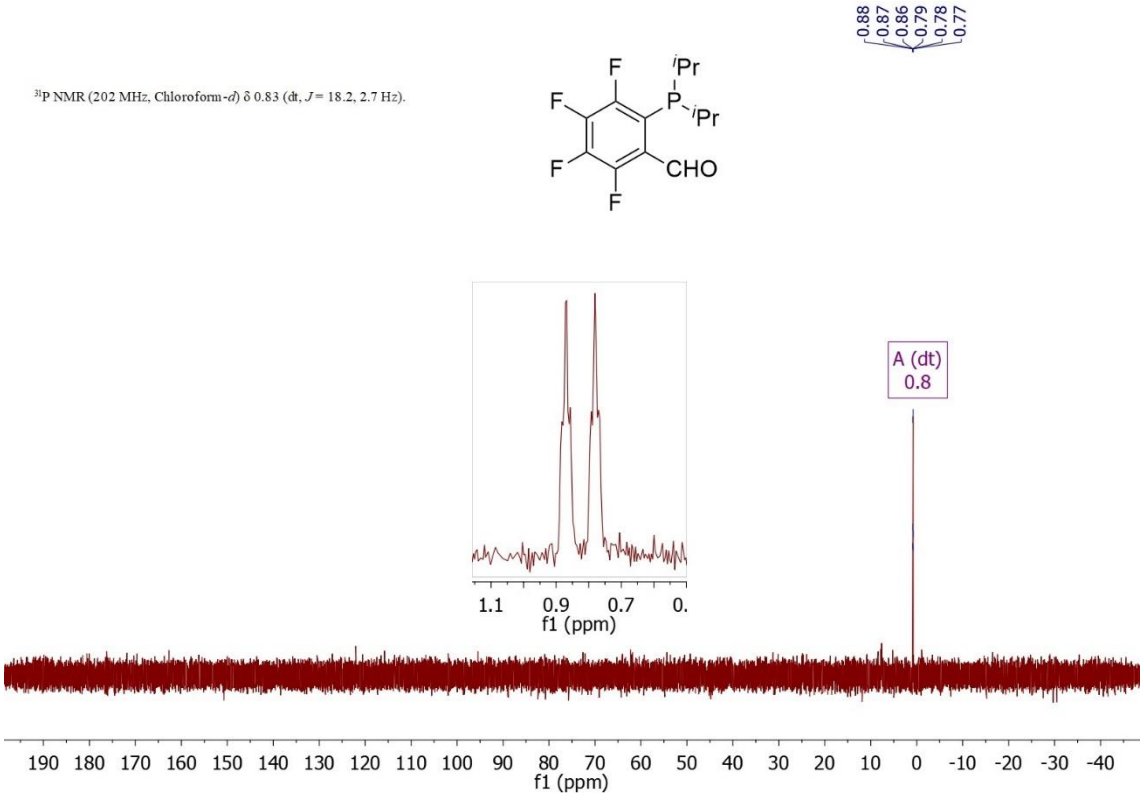

Figure S26. $^{31}P\{^{1}H\}$ NMR of 2-(diisopropylphosphaneyl)-3,4,5,6-tetrafluoro-benzaldehyde.

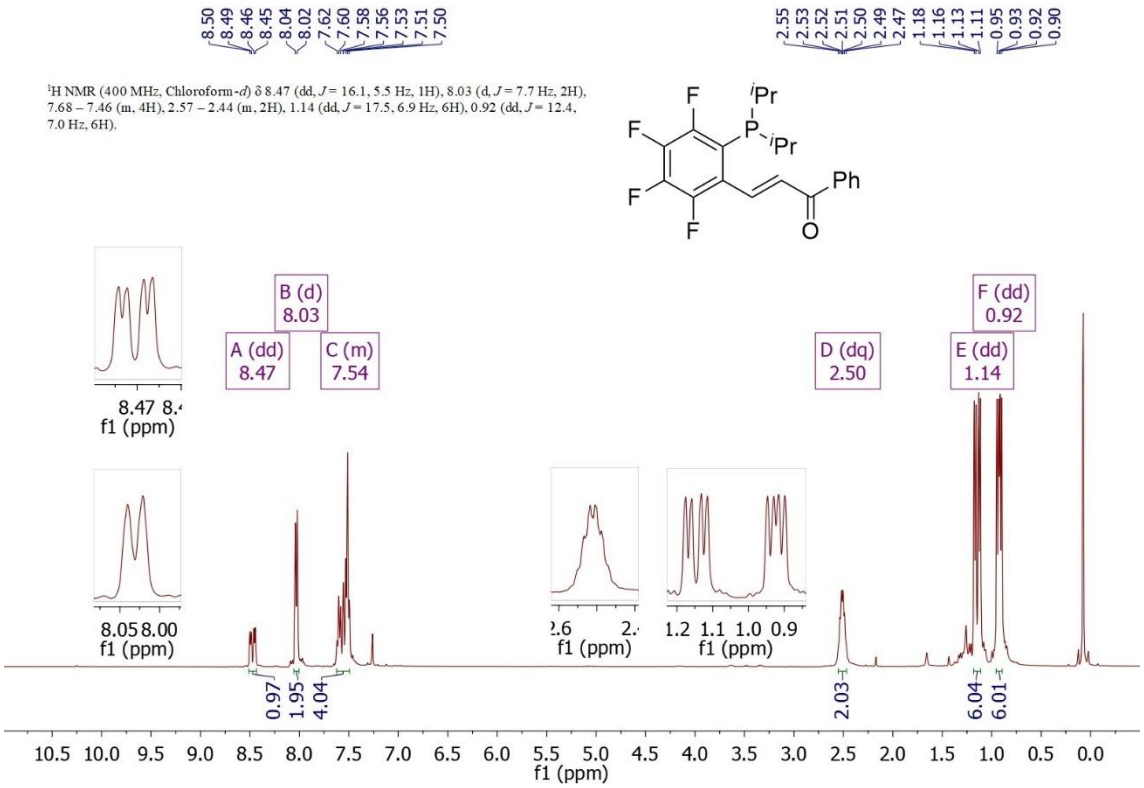

Figure S27. ^{1}H NMR of iPr-PEWO-F_4 (**L^{3}**) in $CDCl_3$.

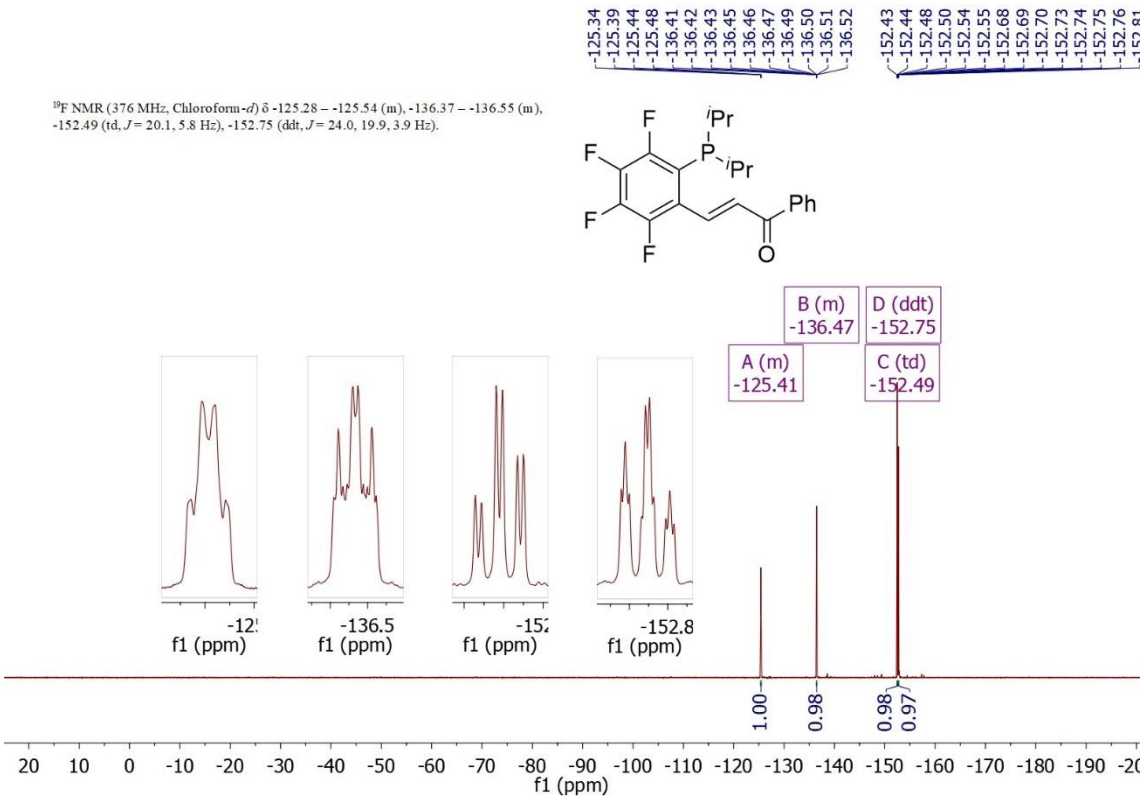

Figure S28. ^{19}F NMR of iPr-PEWO-F_4 (**L^{3}**) in $CDCl_3$.

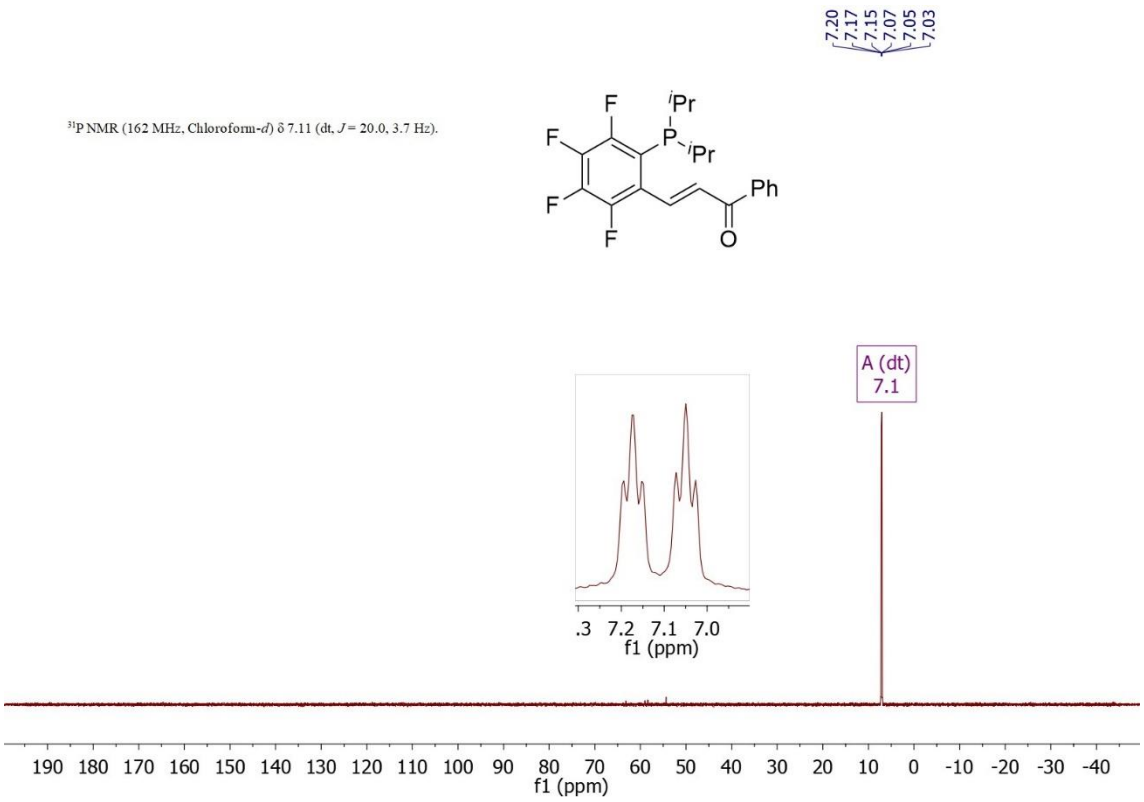

Figure S29. $^{31}P\{^{1}H\}$ NMR of iPr-PEWO-F_4 (**L^3**) in $CDCl_3$.

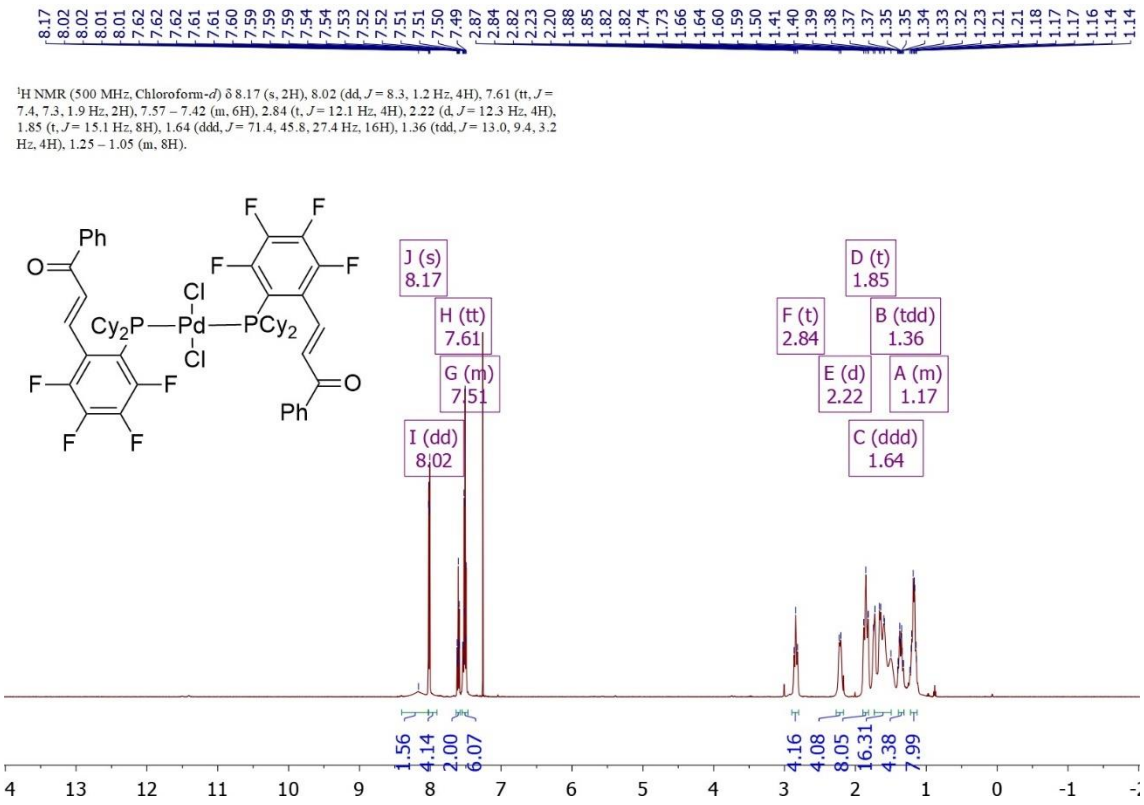

Figure S30. ^{1}H NMR of *trans*-$PdCl_2$(Cy-PEWO-F_4)$_2$ (**1L^2**) in $CDCl_3$.

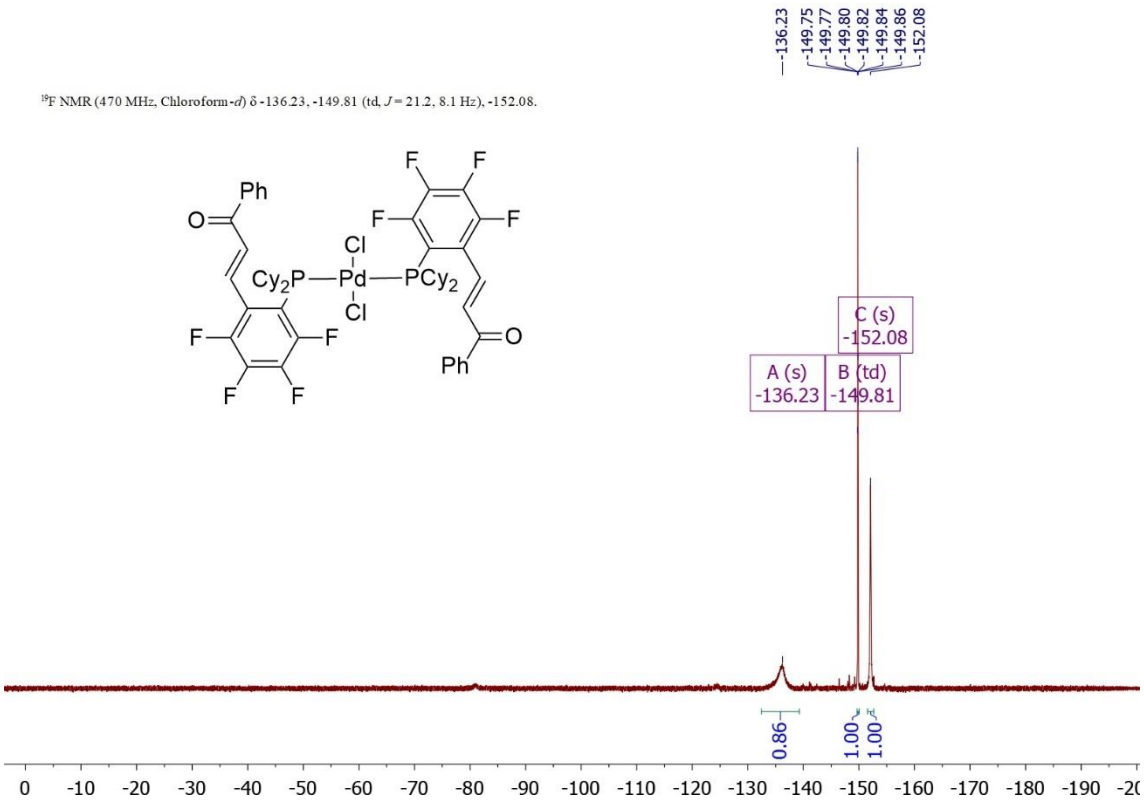

Figure S31. ^{19}F NMR of *trans*-$PdCl_2$(Cy-PEWO-F_4)$_2$ (**1L^2**) in $CDCl_3$.

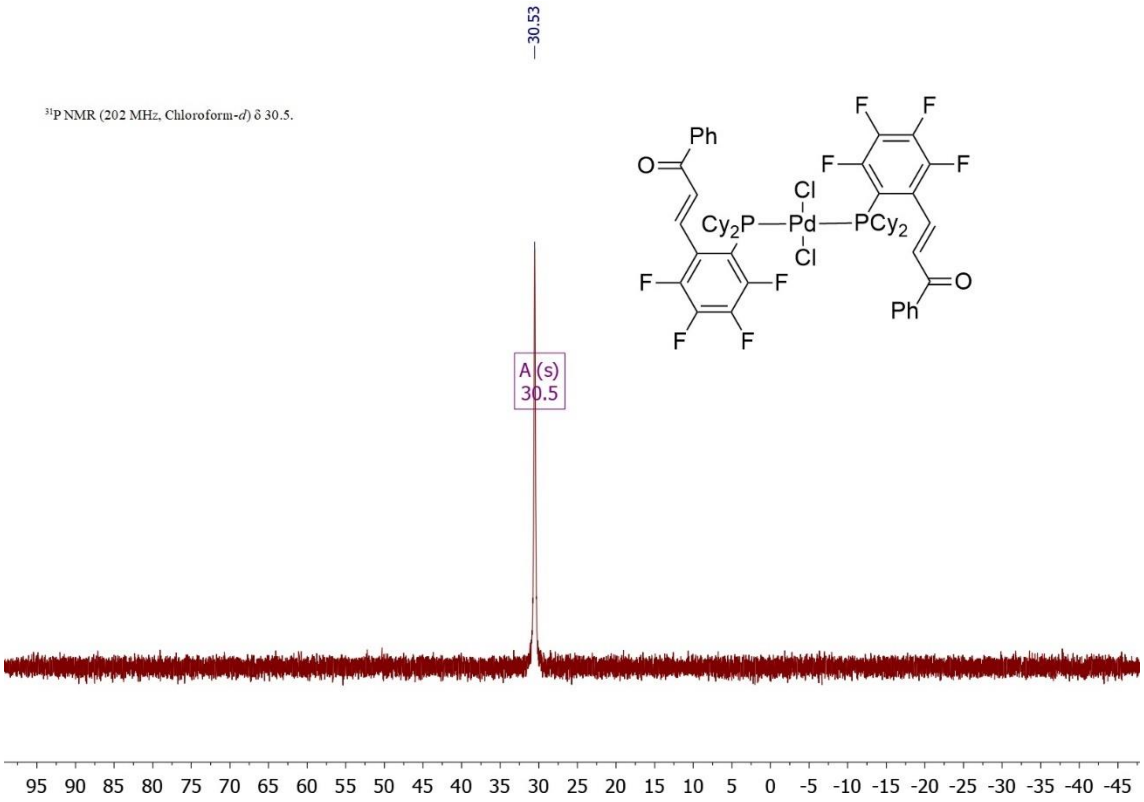

Figure S32. $^{31}P\{^1H\}$ NMR of *trans*-$PdCl_2$(Cy-PEWO-F_4)$_2$ (**1L^2**) in $CDCl_3$.

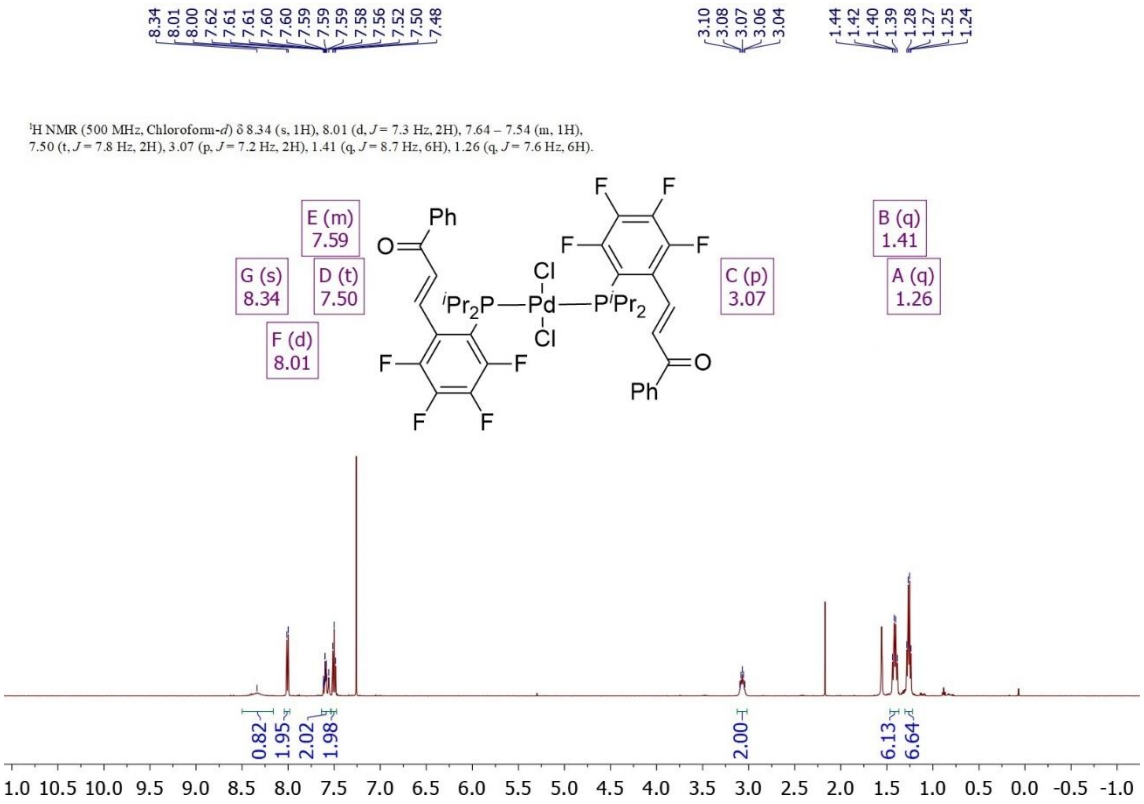

Figure S33. ^{1}H NMR of *trans*-$PdCl_2$(iPr-PEWO-F_4)$_2$ (**1L^3**) in $CDCl_3$.

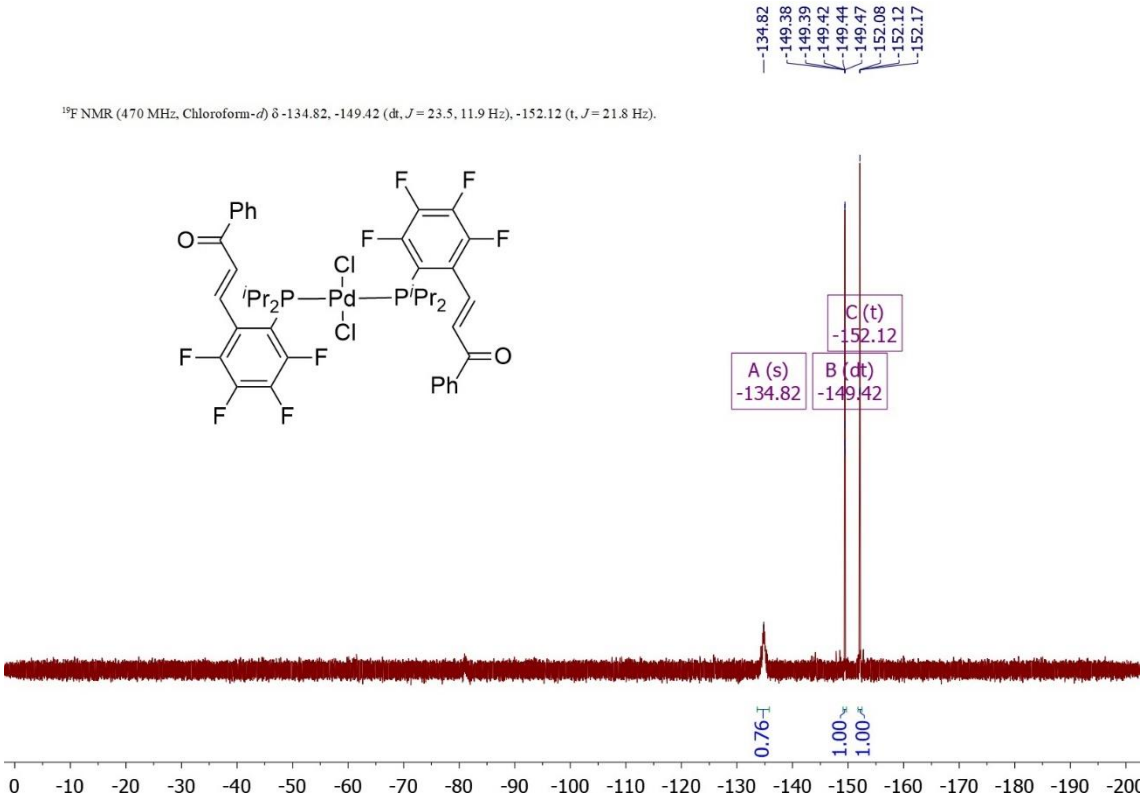

Figure S34. ^{19}F NMR of *trans*-$PdCl_2$(iPr-PEWO-F_4)$_2$ (**1L^3**) in $CDCl_3$.

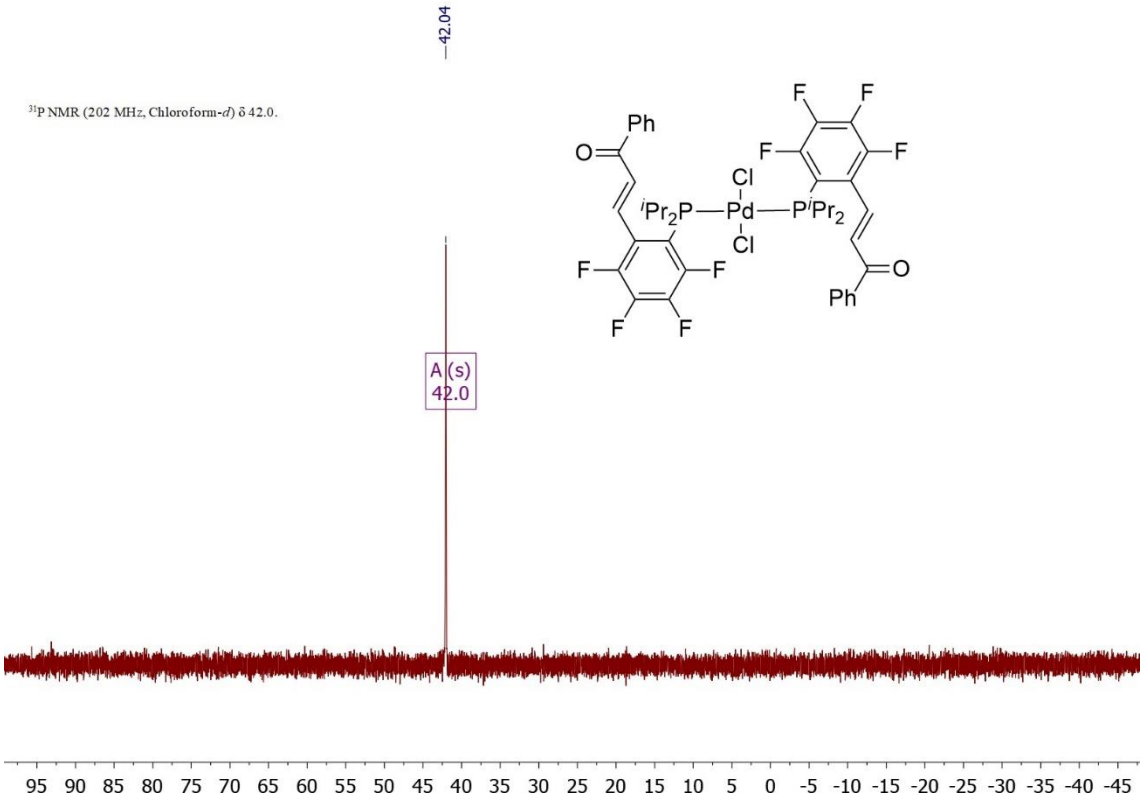

Figure S35. $^{31}P\{^{1}H\}$ NMR of *trans*-$PdCl_2$(iPr-PEWO-F_4)$_2$ (**1L^3**) in $CDCl_3$.

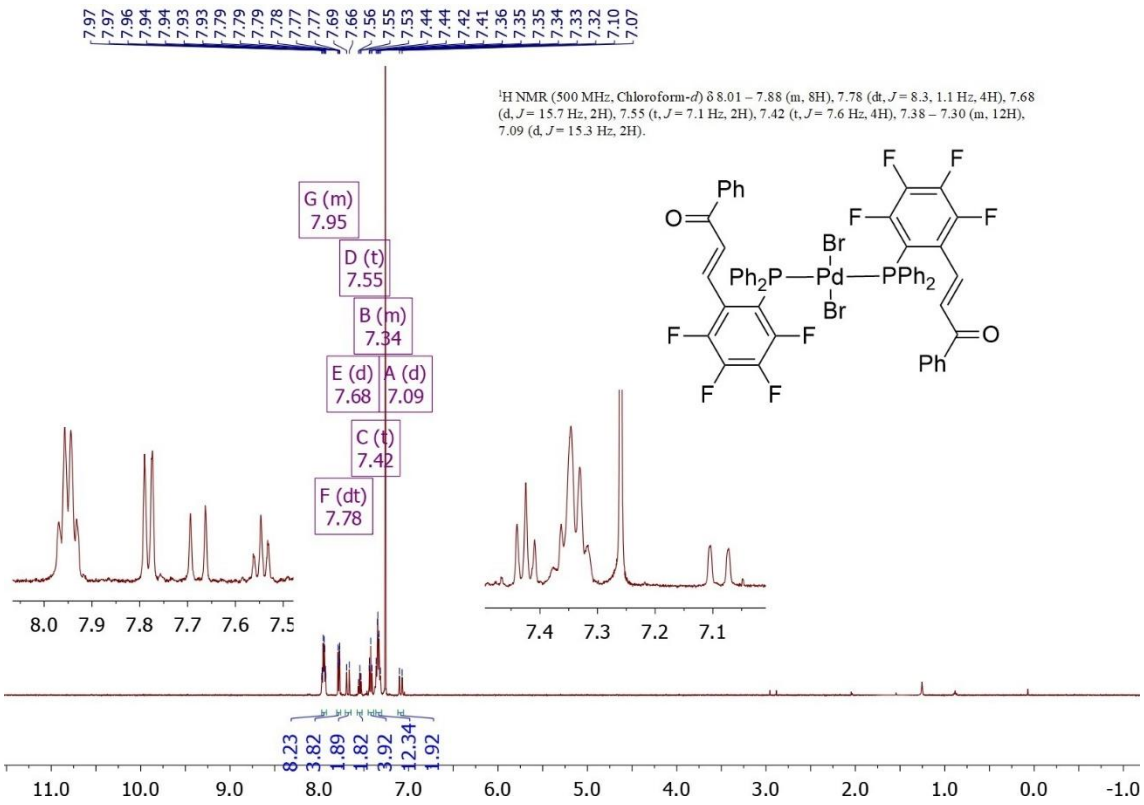

Figure S36. ^{1}H NMR of *trans*-$PdBr_2$(Ph-PEWO-F_4)$_2$ (**3L^1**) in $CDCl_3$.

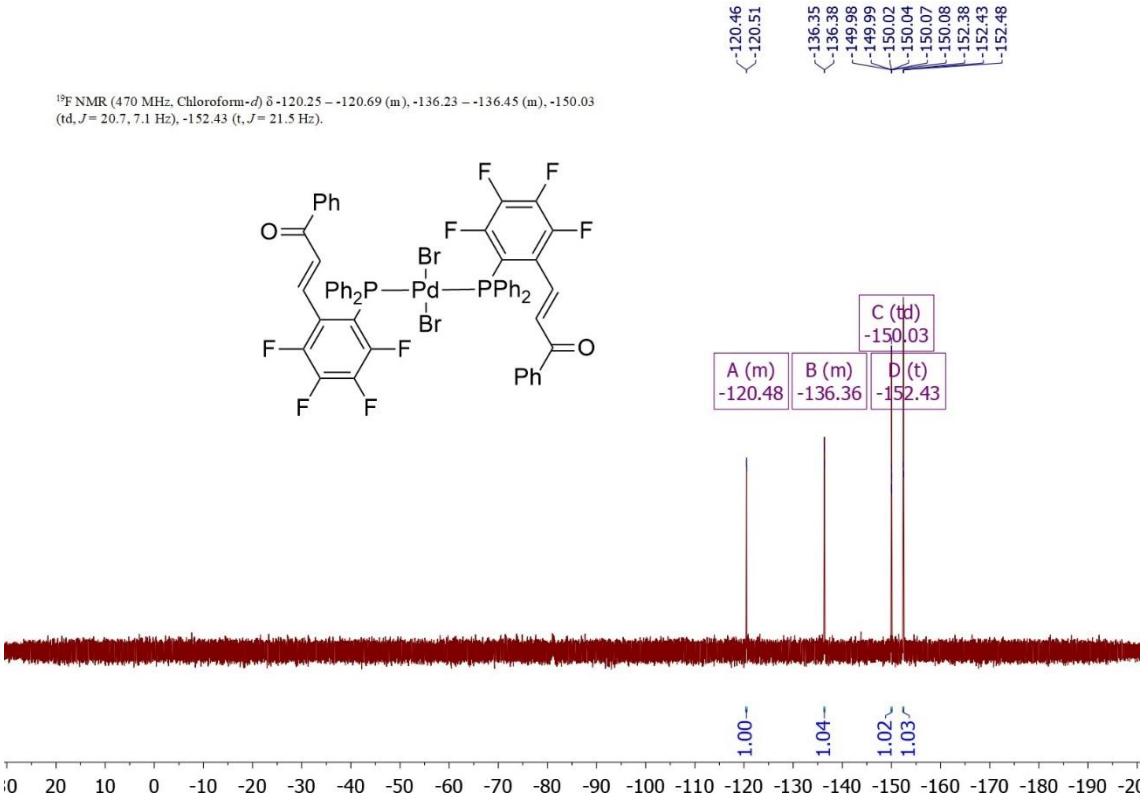

Figure S37. ^{19}F NMR of *trans*-$PdBr_2$(Ph-PEWO-F_4)$_2$ (**3L^1**) in $CDCl_3$.

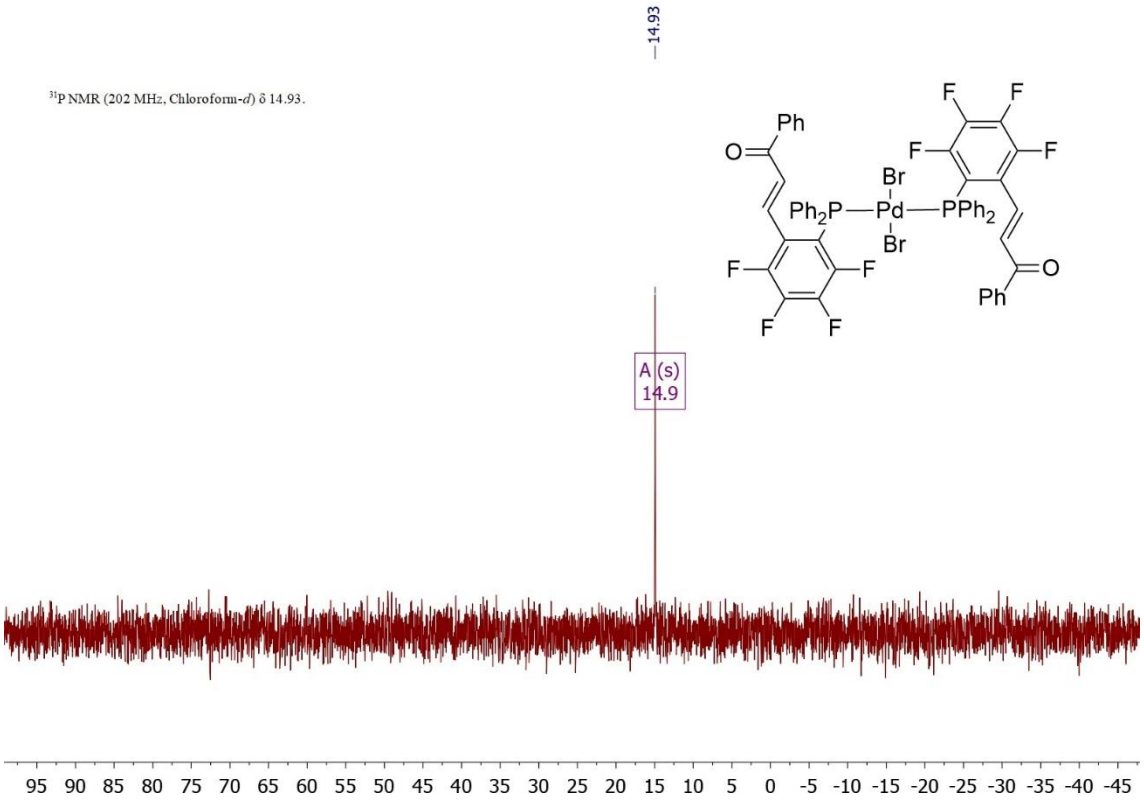

Figure S38. $^{31}P\{^1H\}$ NMR of *trans*-$PdBr_2$(Ph-PEWO-F_4)$_2$ (**3L^1**) in $CDCl_3$.

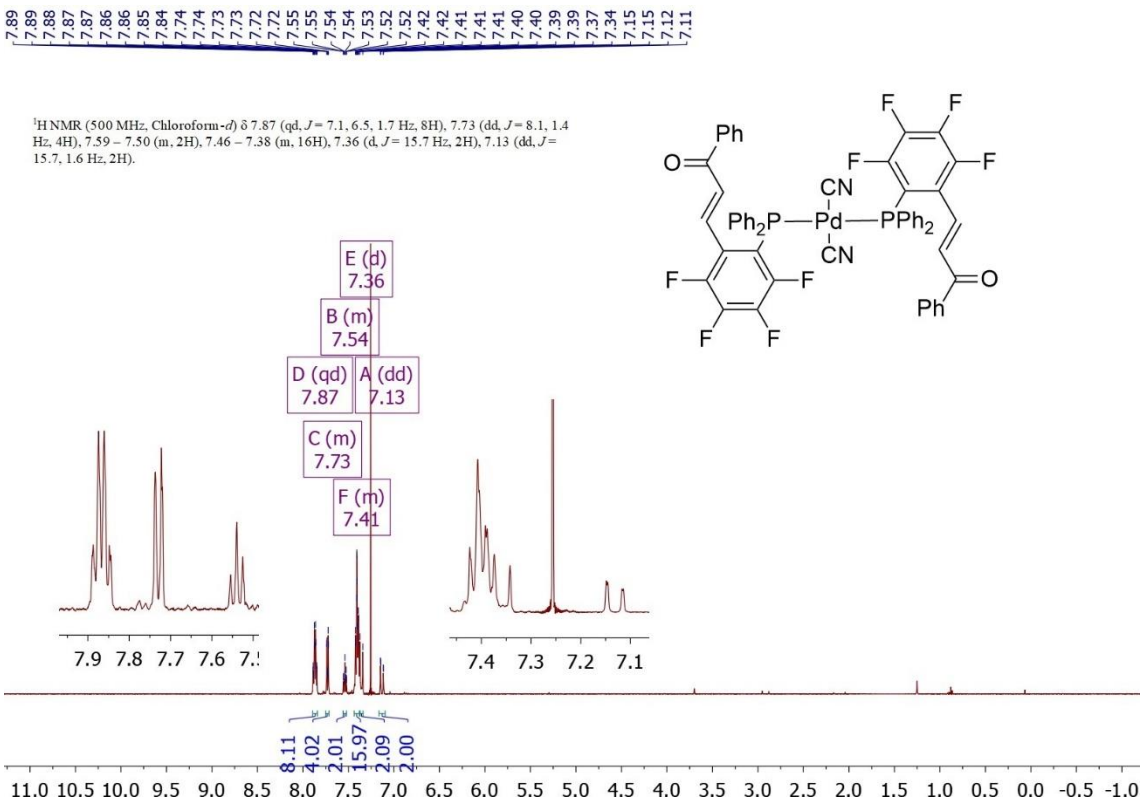

Figure S39. ^{1}H NMR of *trans*-Pd(CN)$_2$(Ph-PEWO-F$_4$)$_2$ (**4L^1**) in CDCl$_3$.

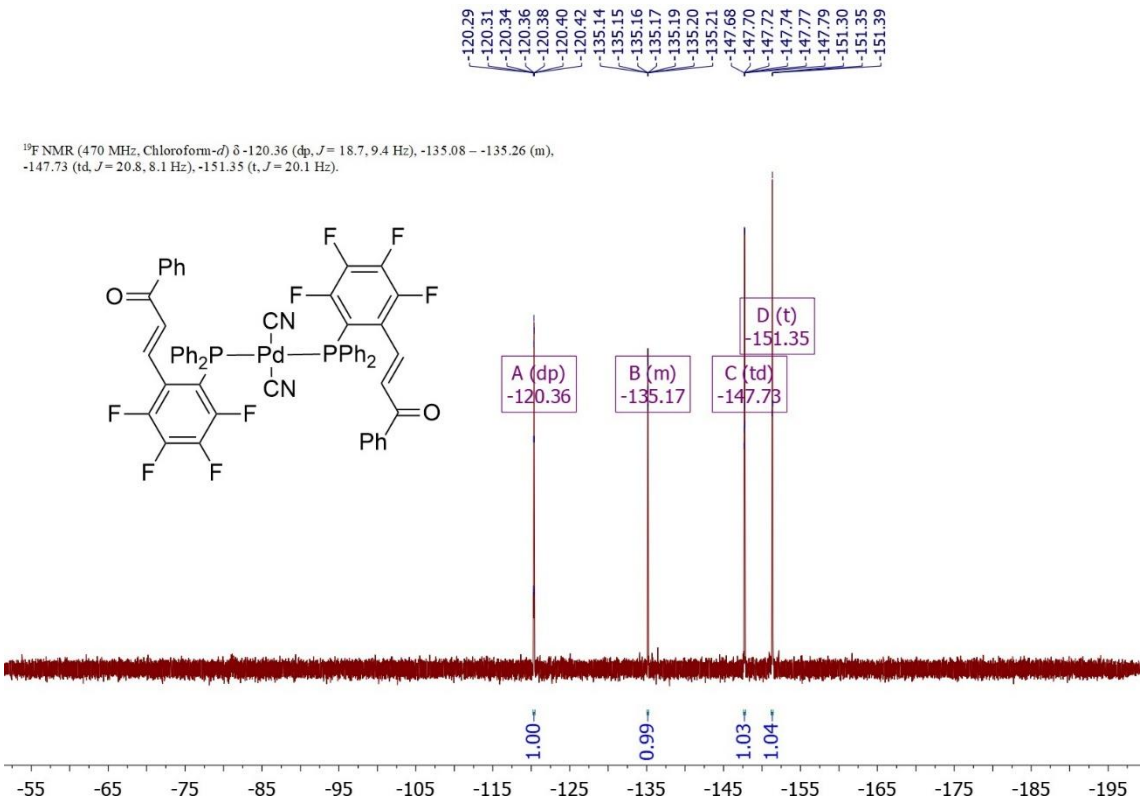

Figure S40. ^{19}F NMR of *trans*-Pd(CN)$_2$(Ph-PEWO-F$_4$)$_2$ (**4L^1**) in CDCl$_3$.

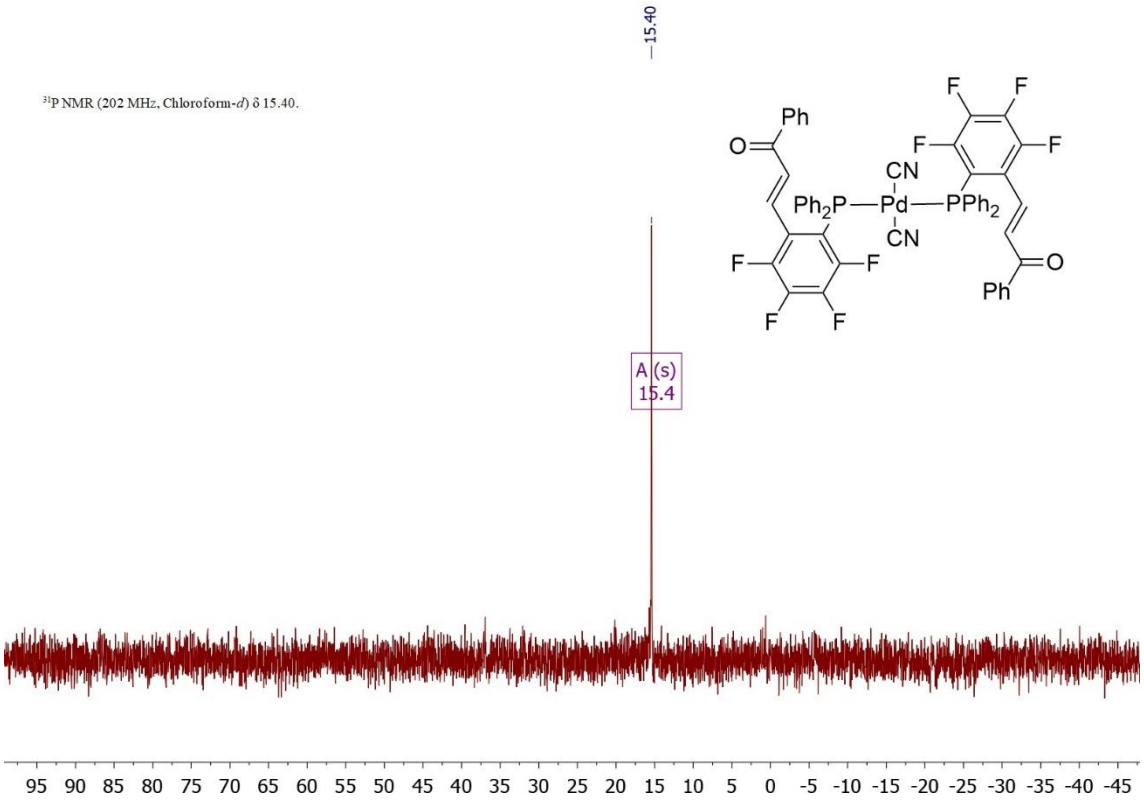

Figure S41. $^{31}P\{^{1}H\}$ NMR of *trans*-$Pd(CN)_2(Ph\text{-}PEWO\text{-}F_4)_2$ (**4L^1**) in $CDCl_3$.

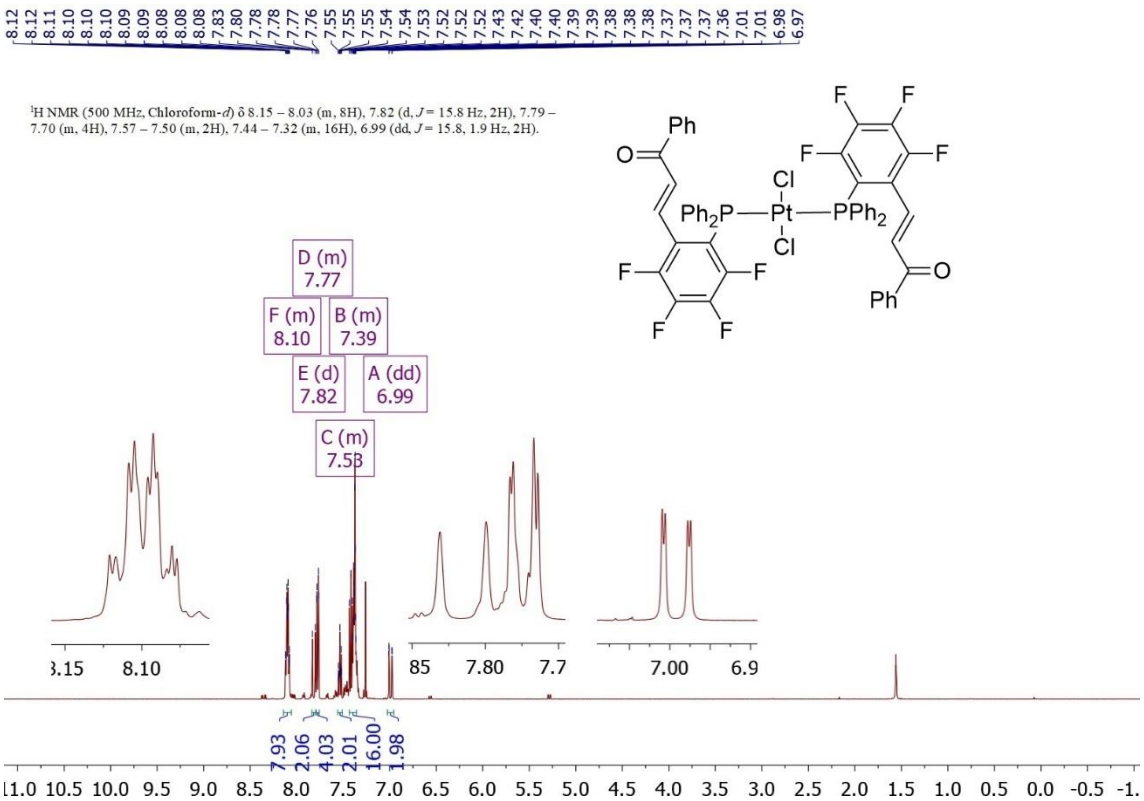

Figure S42. ^{1}H NMR of *trans*-$PtCl_2(Ph\text{-}PEWO\text{-}F_4)_2$ (**5L^1**) in $CDCl_3$.

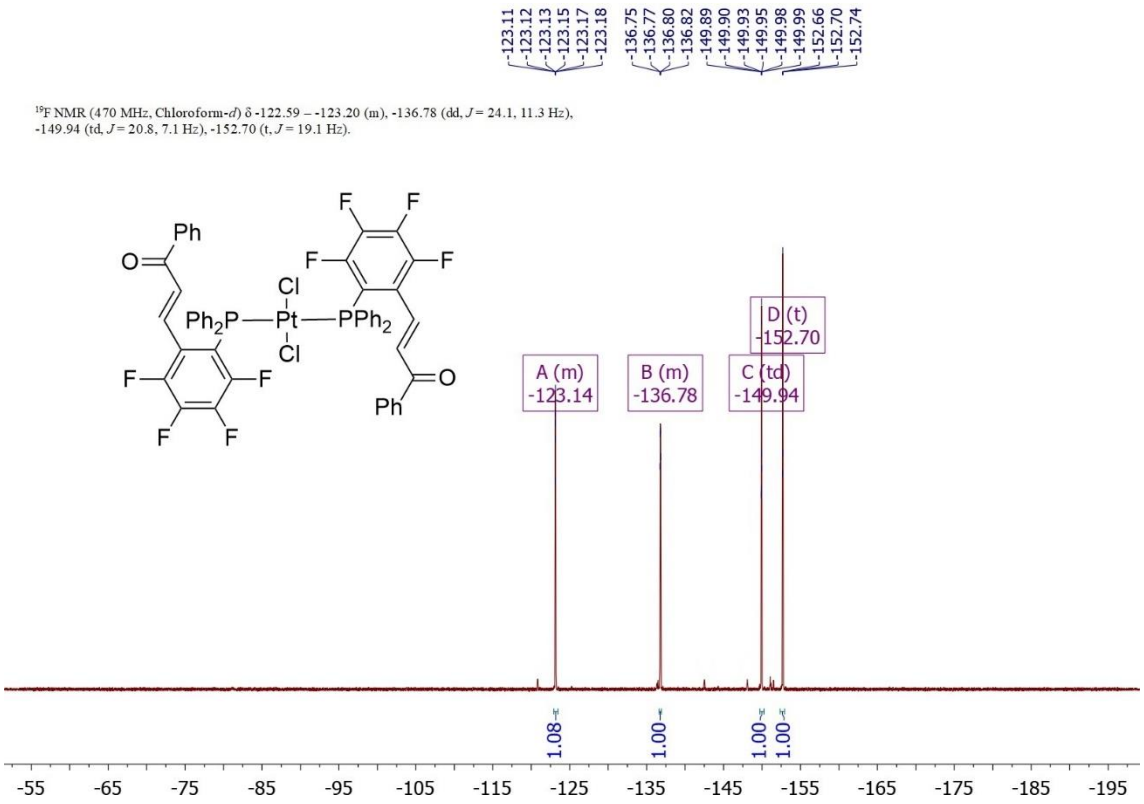

Figure S43. ^{19}F NMR of *trans*-$PtCl_2$(Ph-PEWO-F_4)$_2$ (**5L^1**) in $CDCl_3$.

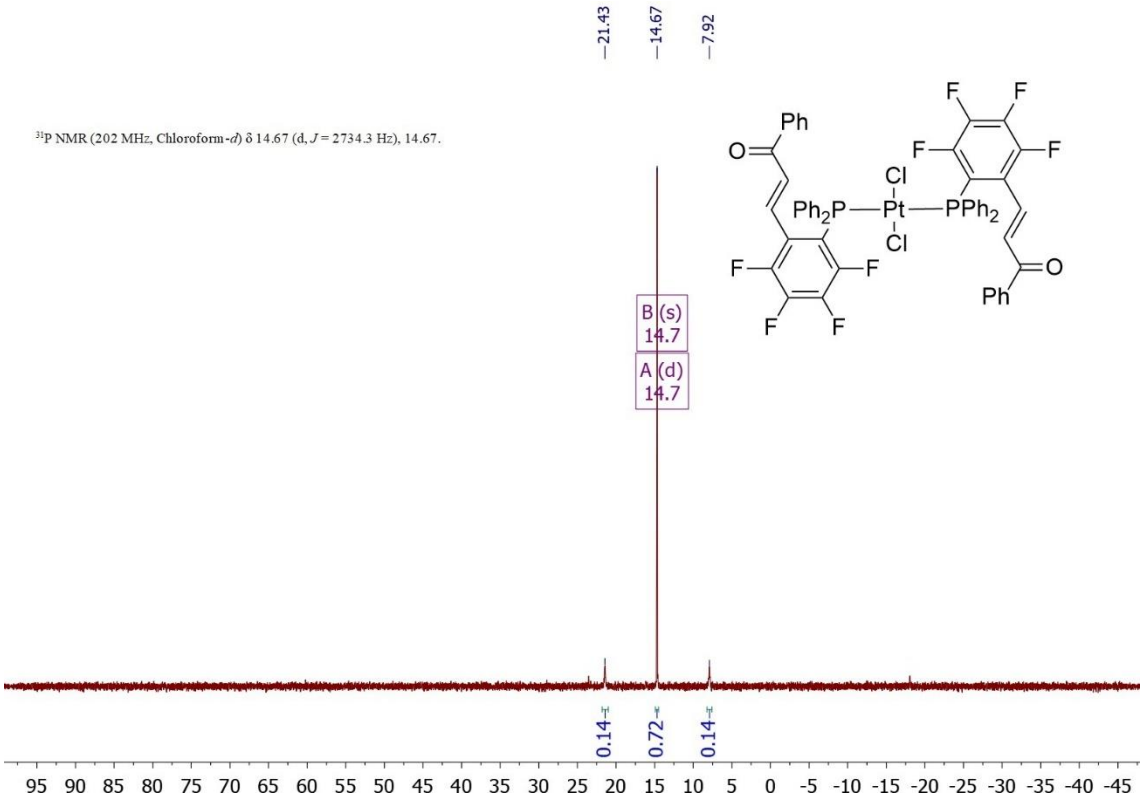

Figure S44. $^{31}P\{^1H\}$ NMR of *trans*-$PtCl_2$(Ph-PEWO-F_4)$_2$ (**5L^1**) in $CDCl_3$.

Fluxionality of $1L^2$ and $1L^3$ complexes

In the ^{19}F NMR spectra of **$1L^2$** and **$1L^3$**, one resonance for each fluorine atom of the R-PEWO-F_4 ligand is expected. However, only 3 resonances are observed at room temperature, one of them being broad. Therefore, ^{19}F NMR spectra of $1L^3$ was also collected at 253 K. At this temperature, a total of 6 resonances are observed, 4 broad signals and 2 singlets with an intensity twice of the broad signals, making a total of 8 fluorine atoms, as expected. Figure S45 shows the ^{19}F NMR spectra of **$1L^3$** at 253 K (bottom) and 298 K (top).

These observations indicate that, in solution, a dynamic process takes place for **$1L^2$** and **$1L^3$**. Coalescence temperature for this process is close to room temperature, which explains why one of the resonances is not observed. When the temperature is lowered, the rate of the process is lowered, and the fluorine resonances are out of coalescence. Hence, they are split in 2 resonances, one for each R-PEWO-F_4 ligand.

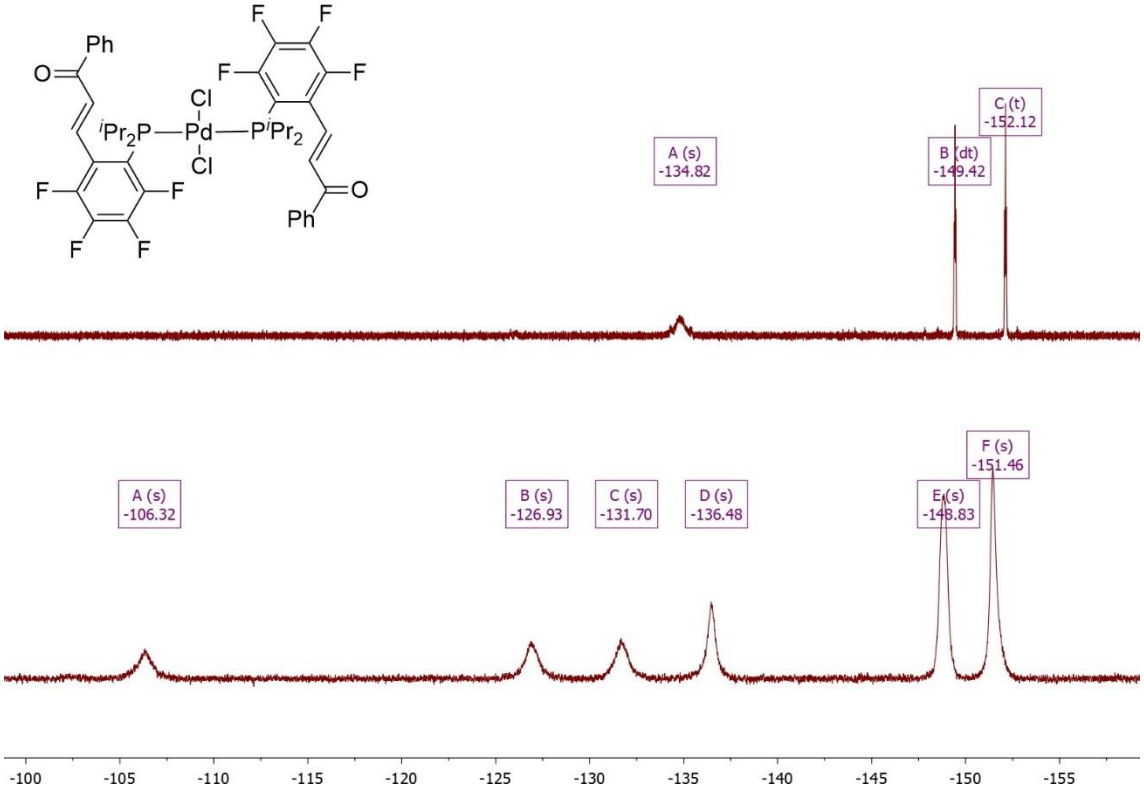

Figure S45. ^{19}F NMR spectra of **$1L^3$** at 253 K (bottom) and 298 K (top).

References

[1] D. B. G. Williams and M. Lawton, *J. Org. Chem.*, 2010, **75**, 8351–8354.

[2] E. Gioria, J. M. Martínez-Ilarduya, D. García-Cuadrado, J. A. Miguel, M. Genov and P. Espinet, *Organometallics*, 2013, **32**, 4255−4261.

[3] M. N. Peñas-Defrutos, A. Vélez, E. Gioria and P. Espinet, *Organometallics* 2019, **38**, 4701−4707.

[4] X. Luo, H. Zhang, H. Duan, Q. Liu, L. Zhu, T. Zhang and A. Lei, *Org. Lett*. 2007, **9**, 4571−4574.

[5] H. Zhang, X. Luo, K. Wongkhan, H. Duan, Q. Li, L. Zhu, J. Wang, A. S. Batsanov, J. A. K. Howard, T. B. Marder and A. Lei, *Chem. - Eur. J.* 2009, **15**, 3823−3829.

[6] CrysAlisPro Software system, version 1.171.33.51, 2009, Oxford Diffraction Ltd, Oxford, UK.

[7] O. V. Dolomanov, L. J. Bourhis, R. J. Gildea, J. A. K. Howard and H. Puschmann, *J. Appl. Crystallogr.*, 2009, **42**, 339–341.

[8] G. M. Sheldrick, *Acta Cryst.,* 2015, **A71**, 3–8.

[9] G. M. Sheldrick, Crystal structure refinement with SHELXL, *Acta Cryst.*, 2015, **C71**, 3–8.

[10] M. J. Frisch, G. W. Trucks, H. B. Schlegel, G. E. Scuseria, M. A. Robb, J. R. Cheeseman, G. Scalmani, V. Barone, B. Mennucci, G. A. Petersson, H. Nakatsuji, M. Caricato, X. Li, H. P. Hratchian, A. F. Izmaylov, J. Bloino, G. Zheng, J. L. Sonnenberg, M. Hada, M. Ehara, K. Toyota, R. Fukuda, J. Hasegawa, M. Ishida, T. Nakajima, Y. Honda, O. Kitao, H. Nakai, T. Vreven, J. A. Montgomery, Jr., J. E. Peralta, F. Ogliaro, M. Bearpark, J. J. Heyd, E. Brothers, K. N. Kudin, V. N. Staroverov, T. Keith, R. Kobayashi, J. Normand, K. Raghavachari, A. Rendell, J. C. Burant, S. S. Iyengar, J. Tomasi, M. Cossi, N. Rega, J. M. Millam, M. Klene, J. E. Knox, J. B. Cross, V. Bakken, C. Adamo, J. Jaramillo, R. Gomperts, R. E. Stratmann, O. Yazyev, A. J. Austin, R. Cammi, C. Pomelli, J. W. Ochterski, R. L. Martin, K. Morokuma, V. G. Zakrzewski, G. A. Voth, P. Salvador, J. J. Dannenberg, S. Dapprich, A. D. Daniels, O. Farkas, J. B. Foresman, J. V. Ortiz, J. Cioslowski and D. J. Fox, *Gaussian 09 (Revission B.1)*; Gaussian Inc.: Wallingford CT 2010.

[11] (a) A. D. Becke, *J. Chem. Phys.,* 1993, **98**, 5648–5652. (b) C. Lee, W. Yang and R. G. Parr, *Phys. Rev. B,* 1988, **37**, 785–789.

[12] P. J. Hay and W. R. Wadt, *J. Chem. Phys.,* 1985, **82**, 299–310.

[13] (a) P. C. Hariharan and J. A. Pople, *Theoret. Chim. Acta,* 1973, **28**, 213–222. (b) M. M. Francl, W. J. Petro, W. J. Hehre, J. S. Binkley, M. S. Gordon, D. J. DeFrees and J. A. Pople, *J. Chem. Phys.,* 1982, **77**, 3654–3665.

[14] M. E. Casida, C. Jamorski, K. C. Casida and D. R. Salahub, *J. Chem. Phys.,* 1998, **108**, 4439–4449.